RSC Advances

ROYAL SOCIETY OF CHEMISTRY

www.rsc.org/advances

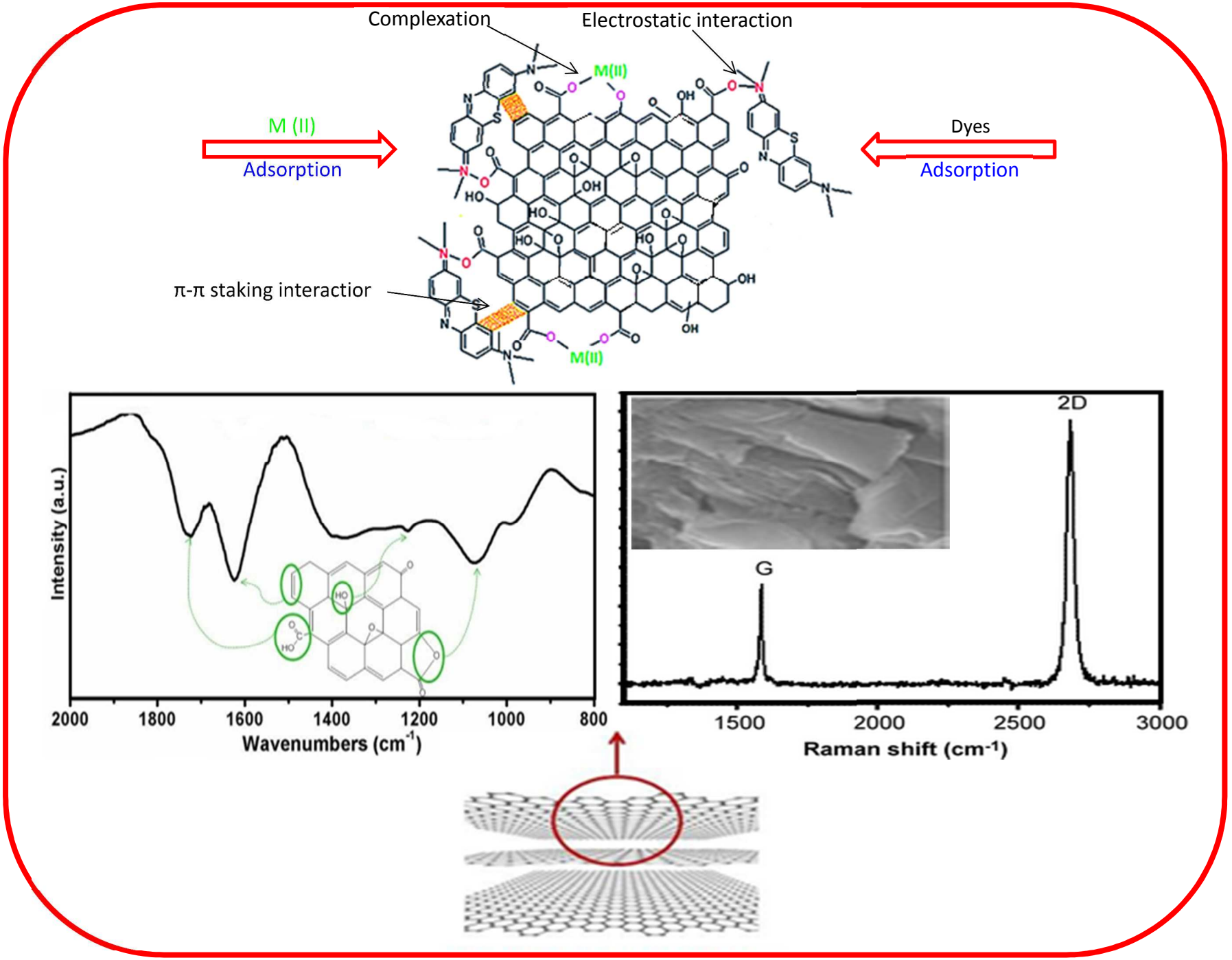

Applications of graphene and its derivatives as an adsorbent for heavy metals and dyes removal: A systematic and comprehensive overview

Mohammed Yusuf[a], F. M. Elfghi [a, b], Shabi Abbas Zaidi[c], E. C. Abdullah [a, b], Moonis Ali Khan[*d]

[a]Malaysia-Japan International Institute of Technology, Department of Environmental Engineering and Green Technology, Jalan Semarak, 54100 Kaula Lumpur, Malaysia.

[b]Chemical Reaction Engineering Group (CREG), Faculty of Chemical and Natural Resources Engineering, University Technology Malaysia, 81310 UTM, Skudai, Johor, Malaysia

[c]Department of Chemistry, Kwangwoon University, Wolgye-dong, Nowon-gu, Seoul, 139-701, Republic of Korea

[d]Advanced Materials Research Chair, Chemistry Department, College of Science, King Saud University, Riyadh, Saudi- Arabia

*Corresponding Author: Moonis Ali Khan
Email: mokhan@ksu.edu.sa; moonisalikhan@gmail.com

Abstract

Because of their persistency and toxicity dyes and heavy metals ions discharged to water bodies have become a worrisome issue. Therefore, to secure the innate beauty of our planet and to conserve our non-renewable natural resources, specifically water; it is essential to check and/or to minimize heavy metal ions and dyes concentration before being discharged. Adsorption is considered as a robust and widely acclaimed water decontamination technology. Graphene, a carbon allotrope with two-dimensional sheet like structure is a latest sensation in material science research. Owing to its unique structural properties, it is a center of attraction for the scientific community for its utilization in various research areas. Here in, we have presented recent developments specifically focusing on the use of graphene and its derivatives as an adsorbent for dyes and heavy metal ions removal from aqueous phase. A historical overview, synthesis methodologies, structural characteristics, and toxicity issues and the applications of graphene and its derivatives for dyes and heavy metal ions removal along with its adsorption mechanism were comprehensively discussed. Major challenges in graphene synthesis and future research perspectives to develop alternate synthesis methodology were discussed.

Keywords: Graphene (G), graphene oxide (GO), reduced graphene oxide (rGO), heavy metal ions, dye, adsorption, and waste water treatment.

Table of contents

1. Introduction

The discharge of industrial, agricultural, domestic, and municipal waste effluents into the water bodies such as rivers, lakes, and ponds have inevitably resulted in an increased flux of toxic pollutants. Among the water pollutants, dyes and heavy metal ions have drawn serious concern as they are non-biodegradable and tend to accumulate in living organisms. Most of these heavy metal ions are highly toxic and some are reported to be suspected human carcinogen.[1] On the other hand, dyes add undesirable color to water resources, preventing the penetration of sunlight, retarding photosynthetic reactions and affecting aquatic life.[2, 3] Most of the dyes molecules have aromatic ring in their structure, which make them highly toxic, non-biodegradable, carcinogenic and mutagenic to both human beings and aquatic life.[4] Hence, it is essential to remove or to minimize the heavy metal ions and dyes to permissible levels before being discharged to water bodies. Various regulatory authorities and environmental protection agencies have enforced stringent regulations to control their discharge into water resources.

A wide array of wastewater treatment techniques such as flocculation[5], membrane filtration[6], solvent extraction[7], biosorption[8], chemical precipitation[9], ion exchange[10], reverse osmosis[11], electrocoagulation[12], cementation[13], electrowinning[14], coagulation[15], and adsorption[16] have been developed for their abatement in potable, municipal, and wastewater as shown in (Fig. 1). Among different technologies, adsorption is considered as a globally acclaimed water treatment technology owing to its versatility, wide applicability, and economic feasibility. Activated carbon (AC), a carbon based material, is considered as a conventional adsorbent for both domestic and industrial water treatment. However, high regeneration cost and fouling of column are the major demerits of using AC as an adsorbent. Therefore, research to explore better alternative carbon based adsorbents is going on. In last decade, nano-carbonaceous materials such as carbon nano-tubes (CNTs) and graphene have grown as promising adsorbents to sequester dyes and heavy metal ions

from aqueous phase. Compared to their counterparts, graphene has shown appreciable fast adsorption kinetics. Furthermore, the production cost of graphene is comparatively lower than the CNTs and other adsorbents (i.e. resins), while their adsorption capacities are similar.[17]

Graphene, a recently explored two-dimensional carbon allotrope is a new addition to carbon research. High electrical conductivity, superior mechanical flexibility, unique high chemical and thermal stability, high surface functionality and large surface area have made graphene a fascinating material for researchers. The adsorption behavior of graphene-based adsorbents has been investigated on different pollutant models.[18 – 21] Numerous studies have also shown the ability of graphene in adsorbing different pollutants from various aqueous samples.[22 – 25] Moreover, graphene can treat multiple pollutants simultaneously with enhanced adsorption capacities.[18] Recently, numerous works have been reported on utilization of graphene and its composite for the removal of dyes and heavy metal ions from aqueous phase, however, to our best of knowledge there is no review reporting recent research done on utilization of graphene and its derivatives as an adsorbent for dyes and heavy metal ions removal. Therefore, in this review, an effort has been made to briefly enlighten history, synthesis, properties, and toxicological effects of graphene. An account on recent developments in use of graphene as an adsorbent for the removal of dyes and heavy metal ions over the years was made comprehensively.

2. Graphene – An overview

2.1. History

Graphene is a parent of all graphitic forms, a two-dimensional carbonaceous material comprising a layer of atoms arranged in six-membered ring. Schafhaeutl, a German scientist in 1840 for the first time reported intercalation and exfoliation of graphite with H_2SO_4 and HNO_3.[26] In an effort to characterize the molecular weight of graphite, Brodie, a British chemist, in 1859, modified

Schafhaeutl method by using oxidant such as $KClO_3$ along with strong acids, resulting not only in intercalation of the layers of graphite, but also in chemical oxidation of its surface, and finally in the formation of graphene oxide (GO).[27] Nearly 40 years later, Brodie's method was modified by Staudenmaier by adding the chlorate salt in multiple aliquots over the course of the reaction.[28] These intercalation and oxidation experiments are the first examples of the delamination of graphite into its constituent lamellae. Moreover, as described below, many of these methods, or modifications thereof, are still used today for the preparation of GO and other chemically modified graphene (CMGs). In 1962, Boehm reported that the chemical reduction of dispersions of GO in dilute alkaline media with hydrazine, hydrogen sulphide, or iron(II) salts produced thin, lamellar carbon that contained only small amounts of hydrogen and oxygen.[29] In 1975, van Bommel and co-workers described the epitaxial sublimation of silicon from single crystals of SiC. At elevated temperatures and under ultrahigh vacuum (UHV; $<10^{-10}$ Torr), monolayered flakes of carbon consistent with the structure of graphene were obtained[30] In 1986, Boehm for the first time standardized a term "graphene" to describe a single atom carbon sheet[31]It has a nearly transparent flat single atom sheet like structure consisting of an individual layer of sp^2 hybridized carbon atoms packed densely in a honeycomb lattice and carbon to carbon molecular bond length of 0.142 nm. It was considered that two-dimensional crystals like graphene were thermodynamically unstable and presumed not to exist under ambient conditions. A breakthrough work for successful isolation and characterization of a mechanically exfoliated graphene monolayer by Nobel laureates Konstantin Novoselov and Andre Geim in 2004 at University of Manchester opened a new dimension to graphene research.[32]

2.2. Properties and structure

Theoretically, graphene has a surface area – 2630 m^2/g [33], high-speed electron mobility – 200,000 cm^2/Vs [34] at a carrier density of ~ 0.77 mg/m^2 [35] in magnitude, and relatively the highest electrical conductivity at room temperature (in a magnitude of 10^6).[36] The strong mechanical properties of graphene, with a Young's modulus of ~ 1100 GPa, [37] and an excellent thermal conductivity of ~ 5000 W/m-k [37, 38] are highly favorable for various applications. Furthermore, graphene has fracture strength of 125 GPa,[39] an optical transmittance of about 97.7% [40], and carrier density – 10^{12} $1/cm^2$.[35] Therefore, it is worth stating that graphene possesses the potential to be used in different applications across many fields.

Graphene is the basic building block for carbon allotropes, including graphite, carbon nanotubes, and fullerenes[1] as depicted in (Fig. 2). Many of these structures can be stacked together to form graphite, which is a three-dimensional (3D) structure of carbon atoms, or a "wrapper" to form fullerenes. The 3D drawing of the graphene lattice structure, as illustrated in (Fig. 3a), is a honey comb net with a unit cell consisting of two triangular sub-lattice A and B and although the honey comb net is not itself a Bravais lattice, it can be represented as a two dimensional triangular Bravais lattice. In the graphene lattice, two sub-lattices of carbon atoms are bonded together with σ bonds, and π orbital of each carbon atom in the lattice contributed to a delocalized network of electrons. The electronic structure of graphene is different from typical 3D materials. Six double cones characterize the Fermi surface of graphene, as shown in (Fig. 3b). The experimental and theoretical studies on graphene have progressed very rapidly since the experimental evidence of 2D structure of graphite by.[41] The thermal instability of 2D crystals, however, prohibits the existence of graphene in its pristine form. The structure of graphene is free of defects because all same kinds of atoms are linked together by strong and flexible bonds; this is the origin of the extraordinary

properties of this material. The first graphite oxide (GO) thin films were produced in early 1960s by Boehm group.[29]A method to produce a uniform single layer of carbon was discovered in 1970's by the sublimation of crystalline silicon carbide (SiC) which left behind a layer of mono-crystalline carbon.[30] Unfortunately, the interaction of this layer with the underlying substrate masked the intriguing properties of isolated graphene, and high processing cost restricted interest in this method. In 1990's, advances in the understanding of various carbon nanostructures, namely nanotube and fullerenes were occurred. Interest in these graphene sister-structures paved a way to device new techniques for the isolation of graphene. Finally, in 2004 researchers were able to isolate and identify graphene by using scotch tape to exfoliate single layers from graphite.[32]

(Fig. 4) displayed chemical structures of various forms of graphene term as graphene family nano-materials (GFNs). GFNs comprise single-layer graphene, few-layer graphene (2 – 10 graphene layers), graphene oxide (GO; normally a single layer structure with various oxygen containing functionalities and less electrical conductivity), reduced graphene oxide (rGO; normally a single layer structure with reduced oxygen containing functionalities with high electrical conductivity), nano-sheets, ultrafine graphite (more than 10 sheets but thickness is below 100 nm), graphene ribbons, and graphene dots. With each of these forms a variety of structures are possible, but it is extremely difficult to fully understand and interpret these structures. For example: In case of GO, it is extremely difficult to describe at the molecular level the type, the degree, and the position of the oxygenated groups introduced during the process of graphite exfoliation.[42] Even more complicated is understanding what happens when GO is transformed under reductive condition.[43, 44]

2.3. Synthesis methodology

Despite the potential benefits of graphene, its widespread use has been impeded due to the challenges in synthesizing graphene from graphite or using bottom-up techniques. However, various synthesis techniques have been proposed as discussed here. The epitaxial growth method of graphene can be achieved by the heating of hexagonal crystals of silicon carbide at 2400K.[45,46] Claire et al.[47] synthesized epitaxial graphene by vacuum graphitization during the thermal decomposition of the silicon carbon at 2400K. Decomposition of the silicon carbon crystal at 1473K results in the formation of millimeter-size continuous graphene planes after the vaporization of silicon.[48, 49] The first highly recognized method used for the preparation of graphene was the mechanical exfoliation (top-down approach) carried out by Novoselov and Co-workers.[32] In this method, highly-oriented pyrolytic graphite was embedded in photo resist material, and adhesive tape was used to successively peel off the layers of graphene. Nowadays, one of the highly used and common technique (i.e. Hummer method/modified Hummer method) is oxidation where graphite is oxidized into graphene oxide (GO) by use of strong acids forming stable solution of GO dispersed in water[50] which can be subsequently reduced either by aqueous reduction agents such as hydrazine.[51, 52] The chemical vapor deposition (CVD) is another interesting technique to synthesize graphene in the presence of a metal substrate and it is typically carried out under ultra-high vacuum and at high temperatures.[53] During this process, a vapor-rich hydrocarbon is heated at approximately 1073K, allowing graphene to deposit on the surface of a metal substrates such as nickel or copper. Finally, the liquid phase exfoliation of graphite has been considered as one of the most feasible approach for industrial production of graphene due its scalability and low cost. This approach typically involves sonication of graphite or graphite oxide powders in solvents. Here, it is noteworthy that there are certain advantages and disadvantages to each method and which are also dependent on the end application, as summarized in (Table 1).

2.4. Toxicity

Discovery of graphene has brought a revolution to material science research. For its development, evaluation of its safety profile and the impact on human health is of primary concern. Studies conducted on graphene and its derivatives reported that they exhibit in vitro toxicity. Among derivatives, GO is considered more biocompatible as it results in less damage and toxicity in human cell due to its greater solubility/dispensability. The most prominent route into the human body lies within the respiratory system. However, GO showed dominant accumulation in lungs for long period of time after being intravenously injected into rats or mice, inducing dose dependent pulmonary toxicity.[54, 55] Furthermore, it has been revealed that GO and aggregated graphene incite a severe and persistent injury in the lungs after direct injection (i.e. 50μg/animal) in the organs of mice.[56] This is not surprising as GO without further surface functionalization is not stable in physiological environments due to the screening of electrostatic charges and non-specific binding protein to GO. After entering the blood stream, the GO agglomerates would be trapped in the lung. The risk of pristine graphene nano-platelets to the respiratory system was also reported.[57] Furthermore, it has been suggested that biological response of graphene will vary depending on number of layers, lateral size, stiffness, hydrophobicity, surface functionalization, and dose etc. On the contrary, there are no plausible reasons pointing out that whether graphene flakes can become airborne and inhaled in a form that is dangerous during use.

3. Graphene – A potential adsorbent

3.1 Characterization

It has been established that graphene is highly potential material for dyes and heavy metals ions removal, hence, various characterization probes such as Raman spectroscopy, Fourier transform infrared spectroscopy (FTIR), X-ray diffraction (XRD), scanning electron microscopy (SEM),

transmission electron microscopy (TEM), thermogravimetric analysis (TGA), X-ray photo-electron (XPS) spectrum have been utilized to enlighten the reasons behind it.

Raman spectroscopy is a quick and non-destruction method which uses monochromatic laser excitation to probe the structure of a material. In Raman spectroscopy of graphene, there are three response peaks of interest corresponding to different vibrational, or phonon modes in the material. These are referred as the G peak (~1580 cm^{-1}), the D peak (~1350 cm^{-1}), and the 2D peak (~2700 cm^{-1}).[58] The D peak appears strongly in disordered graphite, and its intensity is considered to indicate the degree of general graphene disorder. For ordered graphene, the intensity ratio of D/G peaks should be <1%. The 2D peak is a harmonic of the D peak. Wang and co-workers showed that a clear band at 1588 cm^{-1} assigned as G band, is associated with the vibration of sp^2 carbon atoms in graphitic 2D hexagonal lattice. Another single and sharp 2D peak appearing at 2698 cm^{-1} corresponded to graphene with few layers[59] as shown in (Fig. 5a). The interaction of X-rays with a crystalline substance (Phase) resulted to the creation of diffraction pattern. (Fig. 5b) showed the X-Ray Diffraction (XRD) signature of graphene. The analysis revealed a strong and narrow peak at $2\theta = 26.46^{\circ}$ corresponding to the (0 0 2) planes of graphene layers occurring in graphite as reported by.[60] A peak at $2\theta = 44.1$ was also observed corresponding to (1 0 1). Another strong peak at $2\theta = 10.8^{\circ}$ occurred, which suggests structural expansion as oxygen-containing groups incorporated between the graphite during the course of strong oxidation.

FT-IR spectroscopic analysis is a vital tool to characterize both the covalent and non-covalent functionalization of graphene and its derivatives. Characteristic bands at 3430 cm^{-1} due to O–H stretching and at 1610 cm^{-1} for skeletal vibration form graphitic domains of adsorbed water and aromatic domain (C=C), respectively were observed. A peak at 1610 cm^{-1} in graphite shifted to 1625 cm^{-1} in GO due to the presence of electron withdrawing oxygen functionalities. The GO shows some new peaks at 1728 cm^{-1} (C=O stretching), 3406 cm^{-1} (O–H stretching), 1052 cm^{-1} for

C–O stretching. A characteristic peak of hydroxyl group at 3430 cm^{-1} was observed in rGO but with reduced intensity compared to GO. A characteristic epoxide group band at 1052 cm^{-1} of graphite.[61]

SEM is a characterization tool to examine the topography, morphology, composition and crystallographic information of a material.[62] From (Fig. 6a), a thin-layer graphene with spontaneous stacking curls from petal-shaped aggregates was observed. The flocculate in the absence of external forces will remain stable, and it is difficult to separate them from each other. The thickness of graphene was determined accurately by TEM[63] taking large number of images to generate a series of thickness statistic. In (Fig. 6b), the graphene layer stacking disorder is clearly displayed. It is mainly because in the oxidation process, the introduction of the hybrid carbon atoms leads to the disturbances of the planar sp^2 carbon layer. In addition, in order to ensure the thermal stability, the thin layer graphene has prompted its spontaneous staking and wrinkled features.

Stankovich provided the elemental characterization of graphene powder by XPS as shown in (Fig. 6c). The Si_{2p} peak associated with the bonding energy of 99.9 eV represents the bond of silicon with –OH form the graphene, resulting from the partial hydrolysis of molecule during the silylation reaction.[64] The N_{1s} XPS spectrum of graphene contains one peak at 400.6 eV, which is assigned to $N\text{-}C^3_{sp}$. Nitrogen is introduced to the graphene surface during the synthesis and reduction process.[65] The O_{1s} peak at 529.4 eV is assumed to be contributed from the C=O or O=C=OH groups.[66] The C_{1s} (Fig 6c) of graphene contains three components of carbon in C-C at 284.6 eV, the carbon in C-OH at 286.1 eV, and carbonyl carbon (C=O) at 290.6 Ev.[67]

TGA analysis of GO under N_2 atmosphere showed a weight loss below 100°C due to degradation of oxygen containing group.[68] Compared to GO, rGO is thermally more stable due to the removal of large fractions of oxygen containing moieties. The TGA analysis of exfoliated GO, initiator modified GO, and GO/polymeric nanocomposite showed 13% weight loss for GO in temperature range 100 – 800°C attributed to degradation of epoxy, carboxylic and hydroxylic

groups. The observed weight losses for modified GO and GO/polymeric nano-composite were 32 and 56% respectively for aforementioned temperature range.[65]

3.2. Adsorption mechanism

Surface properties such as surface area and pore size distribution influence the adsorption on graphene. A surface area generally affects the adsorption of adsorbate on adsorbent as adsorption capacity of an adsorbent depends largely on the total surface area per unit volume of adsorbate. This includes the specific surface area that is the total internal surface area assigned by the pore size distribution of the adsorbent. When the surface becomes larger it resulted in exposure of the area of active sites exposed to adsorbate during the adsorption. Therefore, to increase the adsorption capacity, the adsorbent should have high porosity and small grain size distribution in order to maximize the total surface area.[69] The graphene showed ultrahigh specific surface and no porosity. In order to improve the adsorption capacity of graphene, introduction of porosity is an efficient and feasible method. Combining other porous materials with graphene can introduce porosity. Zhang et al.[70] combine chitosan-geletin with GO to form ordered porous composites for Cu(II) and Pb(II) adsorption, the composite showed an extremely high adsorbing ability for both metal ions.

The introduction of different functionalities might be another possible route to enhance graphene adsorptive performance as these functional groups play a critical role for the binding adsorbates. Specific functional groups have the ability to form specific bonds with the metal ions. Large surface area and oxygen containing adsorption sites on GO are chiefly responsible for stronger adsorption of organic dyes onto GO. It has been reported that oxide containing acidic functional groups decrease the capacity of the adsorbent for adsorption of metals while hydroxyl functional groups enhanced metal adsorption.[71] The oxidation of graphene to GO can introduce –COOH, –C=O, and –OH functionalities over the surface making GO hydrophilic.[72] The mechanism of heavy metal adsorption has been discussed in the following paragraphs.

The adsorption of Pb(II) and Cd(II) onto the GO showed higher metal uptake attributed to larger surface area and oxygen functionalities on GO.[20] Wu et al [73] reported the adsorption of Cu(II) on GO. Experimental data was fitted to Freundlich model with maximum adsorption capacity of 117.5 mg/g for Cu(II). The adsorption of Cu(II) on GO was attributed to complexation, ion-exchange, and electrostatic attraction as shown by equations below:

Equation 1: $GO - COOH + Cu(II) \longrightarrow GO - COO^{-} - Cu(II) + H^{+}$

Equation 2: $(GO - COOH)_2 + Cu(II) \longrightarrow \begin{matrix} GO - COO^{-} \\ \\ GO - COO^{-} \end{matrix} \Big\rangle Cu(II) + 2H^{+}$

Equation 3: $GO - OH + Cu(II) \longrightarrow GO - O^{-} - Cu(II) + 2H^{+}$

Equation 4: $(GO - OH)_2 + Cu(II) \longrightarrow \begin{matrix} GO - O \\ \\ GO - O \end{matrix} \Big\rangle Cu(II) + 2H^{+}$

The adsorption of Cu(II) and Pb(II) on graphite nano-sheet (GNS)/MnO_2 composite was studied by Ren and coworkers.[74] The maximum adsorption capacities for Cu(II) and Pb(II) were 1637.9 and 793.65 μmol/g, respectively. FT-IR, XPS and XRD studies showed that the adsorption of metal ions on GNS/MnO_2 composite involved formation of tetradendate surface complexes. The oxygen containing surface functional groups including hydroxyl groups (C–OH or Mn–OH) were mainly involved in the adsorption process as shown in the following equations:

Equation 5: $GNS/MnO_2 - OH + M(II) \longrightarrow (GNS/MnO_2 - O - M)^{+} + H^{+}$

Equation 6: $GNS/MnO_2 - O^{-} + M(II) \longrightarrow (GNS/MnO_2 - O - M)^{+}$

Equation 7: $GNS/MnO_2 - OH + M(II) + H_2O \longrightarrow GNS/MnO_2 - OMOH + 2H^{+}$

where, M: metal ion.

Figure 7 displayed linking of N-(trimethoxysilylpropyl) ethylene diamine triacetic acid (EDTA-silane) with the hydroxyl groups on GO surface.[75] High chelation ability of EDTA together with OH and COOH groups present of GO surface greatly enhanced the adsorption of bivalent Pb(II) ions. The adsorption capacity for Pb(II) on EDTA – GO was 479 mg/g.

In case of dye removal, electrostatic attraction between positively charged amino groups and negatively charged oxygen-containing surface groups and π − π interaction between the localized π electrons in the conjugated aromatic rings of the adsorbent and adsorbate molecules are the two most common interactions generally exist between adsorbate (dye) and adsorbent. The rGO has several active sites interacting with the dye molecules: (i) Negatively charged surface-functional groups such as hydroxyl (-OH) and (-COOH) group, (ii) Delocalized π electrons within sp^2 carbon grains interacting with the lone electron pairs of atoms and free electrons in the aromatic rings of the dye molecule. (iii) Oxygen–containing groups available to form bonds with the dye species.[76, 77] Therefore, development of functionalized graphene nano-composites with large surface area and oxygen containing adsorption sites is important for promising environmental applications.

The efficacy of exfoliated graphene oxide (EGO) and rGO was tested for the adsorption of methylene blue (MB), methyl violet (MV), rhodamine B (RB), and orange G (OG) from aqueous phase.[78] G band shifting in Raman spectra (both blue and red shifts) were observed after dyes adsorption. The interaction of cationic (MB and MV) dyes with EGO was electrostatic, while anionic dye (OG) doesn't show any adsorption with EGO. However, RB probably interacts with EGO through both electrostatic and van der Waals forces. Based on the variations in G band position, the charge transferred from MV, RB, and MB to EGO whereas charge transfer from rGO to OG was observed (Fig. 8).

Furthermore, when compared to other carbon based adsorbents, graphene was found to be the best adsorbent for the removal of bisphenol A from water. The adsorption mechanism could be

mainly π-staking interaction as well as hydrogen bond formation.[79] Here, the smooth surface of graphene is an additional advantage with respect to other carbonaceous materials. The interaction of delocalized π-electrons of graphene and benzene ring of the dye, along with the weak Vander Waal forces between hexagonal arrays of carbon atom and aromatic backbones of composite, is mainly responsible for the removal of organic dye especially pararosaniline from water as compared to other adsorbent materials Chen et al.[80] A comparative study of MB adsorption on carbon based adsorbents (activated carbon, GO and CNTs) was conducted.[81] Results showed that the adsorption of MB on carbon based adsorbents was not only because of large surface area, but also π – π electron donor acceptor interactions and electrostatic attraction between cationic dye ions and negatively charged adsorbents which played the critical roles during adsorption. (Fig. 9 and Fig. 10) illustrates the adsorption mechanism of heavy metals and dyes on graphene and its derivatives.

4. Applications

4.1. Heavy metals adsorption on graphene and its derivatives

As mentioned in preceding sections, numerous research reports have appeared on the utilization of graphene, GO, rGO, and their composite for the adsorption of heavy metals. These applications will be discussed in the following sections.

4.1.1. Adsorption on graphene and its composites

Leng et al.[82] examined the possibility of using graphene as an adsorbent for the removal of Sb(III) in aqueous solutions. Batch adsorption experiments were conducted in order to study the effects of operating parameters, such as the initial concentration, pH, and temperature on Sb(III) adsorption. The process appeared to follow the Freundlich isotherm model, rather than the Langmuir isotherm model. Under optimized conditions, the adsorption capacity of graphene for Sb(III) was found to be 10.92 mg/g. The adsorption kinetics data fitted best to pseudo-second-order model, which was able

to express the overall adsorption process and indicated that the rate determining step involved chemisorption. It was observed that the adsorption capacity increased with decreasing metal ion concentrations, and decreased with decreasing temperature. Furthermore, with any increase in pH value above 3.8, an increase in the metal removal efficiency was observed. Moreover, at a pH value greater than 11, the maximum removal efficiency of 99.5% was recorded. Chang et al.[83] on the other hand studied the potential to adsorb Fe(II) and Co(II) from the aqueous solution using graphene through batch adsorption technique. The maximum adsorption capacities were found to be 299.3 and 370 mg/g for Fe(II) and Co(II), respectively. The adsorption processes were governed by the Freundlich isotherm model, while the adsorption kinetics data fitted to pseudo-second-order model.

Huang et al.[84] synthesized graphene nano-sheets (GNSs) in a low-temperature (i.e. exfoliation temperature as low as 473K) followed by chemical exfoliation under a high vacuum condition. Further, GNSs were physically modified at various temperatures (i.e. 773K (500°C)) and 973K (700°C) and were denoted as GNS-500 and GNS-700, respectively. The impact of heat treatment of GNSs surface chemistry and adsorption characteristics was studied. The results showed that GNSs has potential to decrease in Pb(II) metal concentration. The maximum Pb(II) adsorption capacities were 22.42 and 35.47 mg/g for GNS-500 and GNS-700, respectively. Wu et al.[85] tested the adsorptive potential of cetyl-trimethyl ammonium bromide (CTAB) modified graphene for the removal of Cr(VI) from aqueous solution. Introduction of CTAB to the graphene surface resulted in increase in the adsorption capacity. The CTAB, together with the –OH and –COOH ions on the graphene surface resulted into CTAB-infused graphene (CTAB-GN) which performed well for the removal of Cr(VI) form aqueous solutions. The adsorption equilibrium data displayed an excellent fit to the Langmuir isotherm model. The optimum adsorption of Cr(VI) on CTAB-GN was 21.57 mg/g at pH – 2, initial concentration – 50 mg/g, temperature – 298 K,

adsorbent dosage – 0.6 g, agitation speed – 150 rpm, and equilibration time – 40 minutes. The kinetics data fitted well to pseudo-second-order kinetic model, while the thermodynamic assessment indicated that the adsorption was exothermic and spontaneous process.

Ren et al.[74] had studied the adsorption mechanism of Cu(II) and Pb(II) on graphene δ-MnO_2 nano-sheet. The adsorption data fitted well to Langmuir isotherm model revealing monolayer adsorption. The optimum adsorption capacities for Cu(II) and Pb(II) ions were found to be 1620 and 781 μmol/g, respectively with an equilibration time of 3 hrs. Kinetics data was found to obey pseudo-second-order kinetic model, indicating chemisorption process.

Hao et al.[86] investigated the adsorption of Pb(II) ions using SiO_2-graphene. The optimum adsorption capacity was found to be 113.6 mg/g at 25°C, while the maximum percentage removal was 98.82% at pH 6 and contact time of 30 min. The adsorption kinetics obeyed pseudo-second-order model. The adsorption equilibrium data fitted well to the Langmuir isotherm model. The adsorption process was believed to take place by a mono-layer mechanism, on a homogeneous site on the surface of the SiO_2-graphene.

Chemical functionalization of graphene to improve its removal efficiency was reported by Deng and co-workers Deng et al.[87] They adopted a mild, one step electrochemical approach for the preparation of functionalized graphene sheets with assistance of an ionic liquid and water. 1-octyl-3-methylimidazolium hexafluorophosphate (CP8) and potassium hexafluorophosohate (PF6) were used as ionic liquids. The functionalized graphene sheets, thus, obtained were name GNS^{CP8} and GNS^{PF6}, respectively. They studied the adsorption of bivalent Pb(II) and Cd(II) heavy metals onto chemically functionalized GNS^{CP8} and GNS^{PF6}. The adsorption capacities of Pb(II) and Cd(II) on GNS^{CP8} were 74.18 and 30.05 mg/g, at pH 5.1 and pH 6.2, respectively. On the other hand, the adsorption capacities of Pb(II) and Cd(II) on GNS^{PF6} were 406.4 and 73.42 mg/g at pH 5.1 and pH 6.2, respectively. Both processes proved to follow the pseudo-first-order kinetics model. The

isotherm studies data fitted well to both Langmuir and Freundlich isotherm models. A desorption experiment was then considered for GNS^{PF6}, as it displayed a higher adsorption capacity than GNS^{CP8}. Experimental results showed that GNS^{PF6} could be reused for five consecutive cycles without any significant loss in its initial adsorption capacity.

The adsorption of bivalent metal ions [Ag(II), Cu(II), Hg(II), and Pb(II)] in batch mode on graphene-CNT hybrid aerogels (graphene/MWCNTs and graphene/c-MWCNTs) was reported by Sui et al.[88] The experiments were conducted at room temperature, with an initial concentration – 50 mg/L. The maximum adsorption capacities of Pb(II), Hg(II), Ag(II), and Cu(II) by graphene/c-MWCNTs were 104.9, 93.3, 64.0, and 33.8 mg/g, respectively, while the maximum adsorption capacities of the metal ions (in the same order) by graphene/ MWCNTs were 44.5, 75.6, 46.0, and 9.8 mg/g, respectively were obtained. From these results, it could be concluded that the adsorption capacities of metal ions on graphene/c-MWCNTs were significantly higher compared to graphene/ MWCNTs. This might be due to the presence of more oxygen-containing functional groups in the graphene/c-MWCNTs.

Yuan et al.[89] had tested the adsorption of Cr(VI) from aqueous solutions on Mg-Al-layered graphene. Batch adsorption experiment was conducted at pH 2, contact time 24 hr, and initial concentration range 50 – 200 mg/L. The maximum adsorption capacity obtained was 183.82 mg/g. The equilibrium data fitted well with Freundlich isotherm model, while pseudo-second-order kinetic model well described the kinetic data.

Jabeen et al.[90] utilized a synthesized graphene sheet decorated with zero valent iron nano-particles (G-NZVI) for Cr(VI) removal from aqueous solutions. The Cr(VI) containing solution had initial concentrations between 25 and 125 mg/L, pH 4.25, temperature 298 K, and contact time 4 hr. The observed maximum adsorption capacity of Cr(VI) was 162 mg/g. The pore size and surface area of the iron nanoparticles embedded in the graphene sheet played very important roles in the

adsorption process. The adsorption kinetic data was well described by pseudo-second-order model, while the isotherm data was well fitted to the Langmuir isotherm model. It could be deduced that the entire adsorption process was pH dependent.

The use of MnO_2-synthesized graphene nano-sheet/δ-MnO_2 (GNS/MnO_2) composite with a microwave assisted-method was reported by Ren et al.[61] Working with MnO_2 in wastewater treatment has the advantages of being environmental-friendly and cost effective. The adsorption equilibrium, kinetics, and thermodynamics of Ni(II) ions using the composite were investigated under batch experiments. The GNS/MnO_2 provided maximum adsorption capacity of 46.55 mg/g higher than the MnO_2-rGO and pristine graphene nano-sheets. The equilibrium adsorption data showed an excellent fit to Langmuir Isotherm Model and was endothermic in nature. On the other hand, the adsorption kinetic data was best described by pseudo-second-order rate expression. As a result, GNS-MnO_2 was proved to be a great potential substance for desorption and regeneration, with only 9% loss from its initial adsorption capacity.

The infusion of magnetic graphene nanocomposite (MGNC) with core @ double-shelled nano-particle (composed of crystalline iron core, iron oxide inner shell and amorphous Si-S-O compound outer shell) (Graphene/Fe@Fe_2O_3@Si-SO) via a facile thermo-decomposition process, was proved to be efficient in adsorbing Cr(VI) as reported by Zhu et al.[1] The composite recorded maximum adsorption capacity 1.03 mg/g at an initial metal ion concentration 1 g/L and pH 7.0. A high adsorption rate was reported and the adsorption kinetic being aligned to the pseudo-second-order model.

Nandi et al.[91] reported the use of manganese-incorporated iron(III) oxide-graphene magnetic nanocomposite (Graphene/$Mn_x^{2+}Fe_{2-x}^{3+}O_4^{2-}$) for the removal of As(III) from aqueous solutions. From their research, maximum As(III) adsorption (~14.42 mg/g) under the following optimal experimental conditions: pH 7.0, contact time 2.5 hr, temperature 300 K, and initial Fe(III) oxide

concentrations 1-8 mg/L was recorded. It was reported that the equilibrium adsorption process followed the pseudo-second-order kinetic and the equilibrium isotherm data fitted well to the Langmuir isotherm model.

4.1.2. Adsorption on GO and its composite

Apart from graphene, the efficacy of GO as an adsorbent for the removal of heavy metals from aqueous medium was testified. Li et al.[92] carried out a research on the adsorption capability of U(VI) ions from aqueous solutions onto GO. From the experimental results, maximum U(VI) adsorption capacity (229 mg/g) was observed at room temperature, pH 4 and contact time 4 hrs. In addition, the adsorption data revealed that it could be well fitted to the Langmuir isotherm model. However, a rapid decline in U(VI) uptake was observed in the alkaline region. Wu et al.[73] had also tested the adsorption potential of GO for the removal Cu(II) ions from aqueous solutions. The GO displayed a high adsorption capacity of 117.5 mg/g for Cu(II). Regeneration studies revealed appreciably high adsorption potential even after ten consecutive regeneration cycles.

The efficiency of GO to adsorb Zn(II) ions from aqueous solutions was tested by Wang et al.[93]. The amounts of Zn(II) adsorbed onto GO increased with decreased adsorbent doses. The kinetics data fitted well to pseudo-second-order model. At various temperatures, the isotherm adsorption data obtained were well described by the Langmuir model, with maximum mono-layer adsorption capacity - 246 mg/g at the temperature – 293K, pH – 7.0 and initial concentrations 10 – 100 mg/L. The adsorption process was strongly dependent on the pH, but weakly affected by the ionic strength and presence of foreign ions.

The potential of GO for the removal of divalent metal ions of Cu, Pb, Zn, and Cd was investigated by Sitko et al.[94]. The adsorption affinity was found to follow the sequence Pb(II) > Cd(II) > Zn(II) > Cu(II) in a single metal system, but follow the sequence Pb(II) > Cu(II) >> Cd(II) > Zn (II) in a binary metal system. The optimum adsorption capacities for Pb(II), Cd(II), Zn(II), and

Cu(II) were 1119, 530, 345, and 294 mg/g, respectively. The data were well described by the Langmuir isotherm model proving monolayer coverage of heavy metal ions on GO. Whereas, from the kinetics study data, pseudo-second order model applicability was observed. Therefore, the adsorption kinetics of these ions could be controlled by chemisorption, involving strong surface interaction of the metal ions with the oxygen-containing groups on the surface of the GO.

Fang et al.[72] had studied the removal of Co(II) from aqueous solutions by amine modified GO (GO-NH_2). The highest Co(II) removal was 98%, and the maximum adsorption of 116.35 mg/g was observed. The kinetics data was very well described by a pseudo-second-order model. The results showed a dependency of the adsorption mechanism on the adsorbate and adsorbent, and the rate limiting step, representing a chemisorption process involving the valence forces through sharing or exchanging of electrons. Furthermore, the linear regression value showed that the adsorption isotherm fitted the Langmuir isotherm model, suggesting that Co(II) adsorption on the surface of the GO-NH_2 nano-sheets occurred on a surface with homogeneous binding sites with the following principles: 1) equivalent adsorption energies, 2) no interaction between adsorbed species, and 3) mono-layer coverage. Also, an experiment was devised on the parathion of flower-like GO-TiO_2 hybrids for the removal of Zn(II), Cd(II), and Pb(II) from water Lee and Yang.[95] The removal efficiency of these metal ions was significantly improved by the infusion of GO with the flower-like TiO_2 nano-structures. After a period of 6 to 12 hr for hydrothermal treatment at 100°C, the adsorption capacities at pH 5.6 were 44.8 ±3.4 to 88.9 ±3.3 mg/g for Zn(II), 65.1 ±4.4 to 72.8 ±1.6 mg/g for Cd(II), and 45.0 ±3.8 to 65.6 ±2.7 mg/g for Pb(II). In contrast, pristine GO under identical conditions showed much lower removal capacities of 30.1 ±2.5, 14.5 ±1.5, 35.6 ±1.3 mg/g for Zn (II), Cd(II), and Pb(II), respectively.

Recently, Musico et al.[96] had studied the adsorption of Pb(II) using a GO-poly N-vinylcarbazole (PVK) combination to form PV-GO polymer nano-composites. The experiment was

conducted at initial Pb(II) ion concentrations 5 – 300 mg/L, pH 7.0 ±0.5, temperature 298 ±5 K, and contact time 24 hr. The results suggested that the adsorption capacity increased with the amount of GO in the nano-composites. It was explained that the increase in GO concentration led to an increase in the oxygen functionalities availability on the nano-composites. The pH value of the solution played a vital role in the adsorption process, as the increase in pH resulted to increased adsorption efficiency of the nano-composites. From the kinetics studies data, the applicability of pseudo-second-order kinetic model was observed. Additionally, the isotherm equilibrium data fitted well to the Langmuir isotherm model, with the maximum mono-layer adsorption capacity of 887.98 mg/g.

The adsorption capacity of GO was enhanced by introducing the chelating groups to its surface through a silanization reaction between the N-trimethoxysilylpropul ethylenediamine tri acetic acid (EDTA-Silane) and the hydroxyl groups of GO as reported by Madadrang et al.[75] The experiment offered remarkable Pb(II) adsorption capacity of 525 mg/g which is significantly higher than pristine GO (~ 367 mg/g) at pH 6.8, temperature 298±2 K, contact time 24 hr, and initial Pb(II) concentration of 5-300 mg/L. The adsorption kinetic was found to follow pseudo-second-order and the equilibrium data were well described by the Langmuir isotherm model.

The adsorption of Cu(II) from aqueous solutions using GO aerogels was evaluated by Mi et al.[97] The initial Cu(II) ion concentration and pH value played a critical role during this experiment. The optimum adsorption capacity for Cu(II) decreased from 29.59 mg/g (at the temperature of 313K) to 17.73 mg/g (at the temperature of 283K), suggesting endothermic adsorption process. The removal efficiency increased from 32.3 to 96.0% with pH, showing that the adsorption of Cu(II) by GO aerogel was highly pH dependent. Also, the equilibrium data was best fitted to Langmuir isotherm model, indicating that the active binding sites on the adsorbent surface were homogeneous for Cu(II) adsorption. The pseudo-second-order model described the adsorption process and it was

found that the chemical adsorption involving electron exchanges between the adsorbent and adsorbate was dictating the adsorption of Cu(II) onto the GO aerogel.

Cheng et al.[98] conducted a study to determine the adsorption characteristics of U(VI) from aqueous solutions using sepiolite composite-supported GO. The initial U(VI) concentrations tested were 10 - 50 mg/L, and the maximum adsorption capacity of 161.29 mg/g was recorded at pH 5.0 and temperature 298K. Kinetic studies revealed that the process followed pseudo-second-order kinetic model. Furthermore, the process was found to be exothermic in nature, and fitted well with the Langmuir isotherm model.

A study was conducted by Luo et al.[99] to compare the adsorption performances of poly 3-aminopropyltriethoxysilane GO (PAS-GO), 3-aminopropyltriethoxysilane GO (AS-GO), and pristine GO in removing Pb(II) ions from water. The entire process was conducted at a pH 6.0, temperature 303 K, initial concentrations 10 – 400 mg/L, and contact time 7 hr. The maximum Pb(II) adsorption capacities of PAS-GO, AS-GO, and pristine GO at 303 K were 312.5, 119.05, and 204.08 mg/g, respectively. In addition, increase in temperature resulted to an increase in maximum adsorption capacity. From the adsorption isotherm data, it was revealed that the Langmuir isotherm model prevailed, while the adsorption kinetic data followed the pseudo-second-order kinetic model. This study proved that the incorporation of oligomer as cross linkers to fabricate the functional mesh work contributed towards the development of high performance sorbents in removing heavy metal ions from wastewater.

Lei and co-workers[100] had evaluated the adsorption capacities of heavy metals, such as Zn(II), Fe(III), Pb(II), and Cd(II) on foam-infused GO (or GOF). The experiment was initialized at concentration of 50 mg/g for each metal ions. The adsorption isotherm obeyed the Langmuir model, and the resulting optimum adsorption capacities were 252.5, 381.3, 587.6, and 326 mg/g for Cd(II), Pb(II), Fe(III), and Zn(II), respectively. These values were much higher compared to other

conventional carbonaceous adsorbent, such as AC. The adsorption capacities for all the tested heavy metal ions could be sequenced as Fe(III) > Pb(II) > Zn(II) > Cd(II). GOF indicated that the trivalent ion such as Fe(III) may provide a stronger electrostatic force of attraction to the GOF than the bivalent ions. It is also noteworthy that the variation in adsorption capacities for different heavy metals might be due to their unique characteristics as metal ions-functional groups, where some metals tend to be more attracted to certain functional groups.

A poly(amidoamine) modified GO was prepared via grating-from method by Yuan et al.[101] for its potential application in the removal of heavy metal ions such as Fe(III), Cr(III), Zn(II), Cu(II), and Pb(II). The adsorption process was conducted at a constant concentration of 0.0193 mmol/L, contact time of 24 hr, and room temperature. The maximum adsorption capacities for Fe(III), Zn(II), Cu(II), Cr(III), and Pb(II) were 0.5312, 0.2024, 0.1368, 0.0798, and 0.0513 mmol/g, respectively.

An experiment was conducted by Zhao et al.[19] to explore the feasibility of few-layer graphene oxide (FGO) nano-sheets as adsorbents for Co(II) and Cd(II). The adsorption capacities of Co(II) were 167.5 and 68.3 mg/g at temperatures of 333 and 303K, respectively, while, the adsorption capacities of Cd(II) at aforementioned temperatures were 153.6 and 106.3 mg/g, respectively. The isotherm data matched the Langmuir isotherm model. Observations from the experiment showed that the adsorption of Co(II) and Cd(II) on FGO to be weakly dependent on the ionic strength, but rather strongly dependent on the pH value. Consecutively, a thermodynamic study proved the endothermic nature of the process.

Hu et al.[102] had studied the adsorptive potential of sulfonated magnetic GO (SMGO) for the removal of Cu(II) ions from aqueous solutions. They investigated the effect of operating parameters (i.e. pH, initial Cu(II) ions concentration, and temperature) using a response surface methodology (RSM). The maximum adsorption capacity for Cu(II) was 62.73 mg/g at pH 4.68, initial

concentration 73.71 mg/L, and temperature 50°C. The experimental isotherm data obeyed the Langmuir isotherm model, while the adsorption kinetic data followed the pseudo-second-order model. From the thermodynamic data, the adsorption reaction between Cu(II) ions and the active elements on the SMGO was endothermic and spontaneous. In conclusion, SMGO is found to be a promising adsorbent for effective removal of Cu(II) ions from wastewater.

Luo et al.[103] examined the potential of GO-hydrated zirconium oxide nano-composites for As(III) and As(V) removal from wastewater. Based on the results, adsorption capacity of As(III) was slightly higher (95.15 mg/g) than that of As(V), which was 84.89 mg/g. Pseudo-second-order kinetic model gave the best fit with the process occurring at a very fast adsorption rate attaining equilibrium within 15 minutes. Moreover, the equilibrium data agreed with the Langmuir isotherm model. On the other hand, Zhang et al.[104] performed an experiment to determine the adsorption performance of GO/ferric hydroxide to remove As(V) from aqueous solutions. The maximum adsorption capacity was achieved to be 23.78 mg/g.

Liu et al.[105] had examined the magnetite/GO (M-GO) composite to adsorb Co(II) ions from wastewater. The adsorption capacity of Co(II) was determined by varying the temperatures: 303.15, 323.5, and 343.15 K; the corresponding capacities of 12.98, 17.58 and 22.70 mg/g were observed, respectively. The adsorption isotherm data revealed that the reaction was an endothermic and spontaneous process. Both Langmuir isotherm model and pseudo-second-order kinetic fitted well.

To investigate the adsorption of Cr(VI) from aqueous solutions, fabrication of polypyrrole/GO (Ppy/GO) nano-sheets by using sacrificial-template polymerization method was studied by Li group.[106] The optimum adsorption capacity 9.56 mmol/g was obtained for Cr(VI) with as-synthesized adsobent. From this research, observations proved that the experimental data had a good fit with the Langmuir isotherm model and the equilibrium data displayed pseudo-second-order kinetic model.

Peng et al.[107] performed an experiment on GO-FeOOH composite to test the adsorption effectiveness of As(V) from water. The adsorption process was carried out at a temperature 298K as. The synthesized composite portrayed excellent adsorption properties, while the equilibrium study could be well described by the pseudo-second-order kinetic model; while the isotherm data fit well with the Langmuir isotherm model.

The use of synthesized magnetic graphene/iron oxide composite (Fe_3O_4/GO) for the removal of U(VI) from aqueous solutions was recently reported by Zong et al.[108] The optimum U(VI) adsorption capacity on Fe_3O_4/GO at temperature – 293K and pH – 5.5 ±0.1 was 69.49 mg/g. The Langmuir isotherm model and pseudo-second-order kinetic equation both governed the equilibrium and kinetic data, respectively.

Yu et al. [109] had examined the adsorption behavior of Cu(II) ions on GO chitosan aerogel. The observed adsorption capacity was 0.254 mg/g at a temperature 303K, initial concentration 19.2 mg/L, and pH 6.0. In this experiment, the value of pH played an important role on the adsorption performance, an increase in pH value above 6.0 would precipitate the Cu(II) ions. The adsorption kinetic followed the pseudo-second-order model, while the adsorption isotherms were slightly better fitted by the Langmuir isotherm model than the Freundlich Isotherm Model (with an R^2 values: 0.993, and 0.989, respectively).

On the other hand, the removal capability of Pb(II) by porous GO/chitosan (PGOC) composite was studied by He et al.[110] The recorded maximum adsorption capacity was 99 mg/g. In another variation of the study, Liu et al.[23] reported on the use of chitosan/GO (CSGO) composite as the adsorbent for the removal of Au(III) and Pb(II) from aqueous solutions in a batch system. Optimum adsorption capacity values recorded for Au(III) and Pb(II) were 1076.64 mg/g and 216.920 mg/g, respectively. The adsorption kinetics for both ions followed the pseudo-second-order

kinetic model. Also, the chemical adsorption process was a rate-limiting step process, and the experimental data was well interpreted by the Langmuir isotherm model.

Chen et al.[111] performed an experiment to study an effective removal of Cu(II) and Pb(II) from aqueous solutions by using GO-chitosan hydrogen composite. The adsorption process was performed at initial concentration range between 0 and 120 mg/L and temperature 294 ±1K; however, the pH value and contact time were varied. For Cu(II), pH 5.1 and contact time 10 hr were set whereas, for Pb(II), pH 4.9 and contact time 4 hr were used. The adsorption isotherm data for both metal ions agreed to Freundlich isotherm model.

The use of magnetic chitosan/GO composite (MCGO) as a versatile adsorbent for Pb(II) oxide removal from aqueous solutions was reported by Fan et al.[112] The experiment was set at pH 2, contact time 1 hr, initial concentrations range 0 – 120 mg/L, and temperature 303.0 ±0.2K. The experiment proved that the magnetic adsorbent was stable and environmental friendly, with a high adsorption capacity (76.94 mg/g) and an extremely high desorption (90.3%).

Li et al.[113] conducted an experiment on an easy chemical bonding method to synthesize magnetic cyclodextrin-chitosan/GO (CCGO). They investigated the adsorption behaviors of Cr(IV) in aqueous solutions at different temperatures (303, 313 and 323K), while maintaining constant pH 3 and initial concentration 50 mg/L. The maximum adsorption capacities at these temperatures (303 to 323K) were recorded as 61.31, 67.34, and 67.66 mg/g, respectively. These results proved that at higher temperatures, higher adsorption capacity values could be expected. The Langmuir isotherm model exhibited a better fit to the adsorption equilibrium data than the Freundlich isotherm model, implying that a monolayer coverage of Cr(VI) ions onto the composite surface. The adsorption kinetic data followed the pseudo-second-order kinetic model.

Algothmi [114] had reported the use of calcium alginate-GO (Ca-Aig$_2$/GO) hybrid gel beads for effective removal of Cu(II) from aqueous solutions. The maximum Cu(II) uptake of 60.24 mg/g

was observed at room temperature and contact time 1.5 hr. The pseudo-second order rate equation provided a very good fit to the experimental kinetic data and the Langmuir isotherm model to the equilibrium isotherm data.

4.1.3. Adsorption on rGO and its composites

Yang et al.[115] conducted a research on the effect of humic acid (HA) addition onto Cu(II) adsorption process involving few-layered reduced GO (FrGO) and few-layered GO (FGO) using batch equilibrium method. Two separate adsorption experiments were conducted: Experiment #1 without the HA, and Experiment #2 with the addition of the HA. For Experiment #1, results showed that the adsorption capacities of Cu(II) on FrGO and FGO were 11.40 and 73.36 mg/g, respectively. This suggested that FGO was more effective due to its numerous oxygen-containing functional groups. Experiment #2 showed that when HA was added, the adsorption capacity of FrGO increased with increasing initial HA concentrations (from 0.0 to 30.0 mg/L). The increase in the adsorption by FrGO from 11.40 to 18.60 mg/g suggested that the addition HA facilitated the adsorption of Cu(II) as well as followed a pseudo-second-order kinetic model. Also, the adsorption isotherms could be simulated by the Langmuir isotherm model.

In an experiment, Li et al.[116] had explored an effective adsorbent in the form of polyaniline and rGO (PANI-rGO), which was prepared through the polymerization of aniline in the presence of GO to remove Hg(II) from aqueous solutions. The experiment was carried out at initial concentration range 10 – 40 mg/L, pH 4.0, temperature 305K, and contact time 5 hr. The maximum calculated Hg(II) adsorption capacity was 1000 mg/g. The equilibrium adsorption data was well fitted to both Langmuir and Freundlich isotherm models and the adsorption process was well described by pseudo-second-order kinetic model. A low adsorption capacity was recorded at a low pH, which was due to the protonation at the adsorbent surface functional groups, and also due to the lower attachment of Hg(II) on PANI-rGO surface.

The use of synthesized iron-iron oxide matrix dispersed on rGO (rGO-FeO-Fe_3O_4) for As(III) adsorption from aqueous solutions was utilized by Bhunia et al.[117] They had compared the removal capability of As(III) by different adsorbents: (1) rGO-FeO, (2) rGO-Fe_3O_4, and 3) rGO-FeO/Fe_3O_4 at pH 7.0, initial concentration 2.6 mg/L, and contact time 1 hrs. The maximum adsorption capacities recorded were 37.3, 21.2, and 44.4 mg/g for rGO-FeO, rGO-Fe_3O_4, and rGO-FeO/Fe_3O_4, respectively. The adsorption process appeared to follow the Langmuir isotherm model and the adsorption kinetic data to follow the pseudo-second-order model. Furthermore, because of its extremely high adsorption potential, rGO-FeO/Fe_3O_4 was further satisfactorily tested for the removal of metal ions like Cr(III), Hg(III), Pb(II), and Cd(II). The adsorption process was conducted under aforementioned experimental conditions. This process fitted well Langmuir isotherm model. The maximum adsorption capacities recorded were 31.1, 22.0, 19.7, and 1.91 mg/g for Cr(II), Hg(II), Pb(II) and Cd(II), respectively.

The removal of As(III) and As(V) from aqueous solutions using nano-scale zero valent iron-RGO (NZVI-RGO) modified composite was conducted by Wang et al.[118] The experimental conditions for the adsorption were temperature 303K, and contact time 2 hr. However, for As(III), the initial concentration was 3 mg/L, and pH ranged from 4.0 to 10.0, while for As(V), the initial concentration was 8 mg/L, and pH was 2. It was found that the solution pH played a major role in achieving the maximum adsorption. The optimum pH value for the removal of As(V) was 2, while for As (III), the pH values ranged between 4 and 10. The adsorption capacities obtained for As(III) and As (V) were 35.83 and 29.04 mg/g, respectively. The isotherm studies indicated that the adsorption data was better fitted to Langmuir isotherm model ($R^2 > 0.995$) than the Freundlich isotherm model ($R^2 > 0.87$). Moreover, from calculations, the pseudo-second-order kinetic model was deemed a better fit to the experimental kinetic data, rather than the pseudo-first-order kinetic model.

Zhang et al.[119] had developed a magnetic cobalt ferrite – rGO nano-composites ($CoFe_2O_4$-RGO) for the removal of Pb(II) and Hg(II) from aqueous solutions. Batch adsorption experiment was conducted under the following conditions: pH 5.3 and initial concentration 20 mg/L for Pb(II); and pH 4.6 and initial concentration 5 mg/L for Hg(II), temperature 298 K and contact time 2 hr were kept constant for both analytes. The adsorption kinetic and adsorption isotherm were governed by the pseudo-second-order kinetic model and Langmuir isotherm model, respectively. In addition, the used $CoFe_2O_4$-RGO, together with the adsorbed heavy metal ions could be simply recovered from both the wastewater and aqueous solutions with magnetic separation at a very low magnetic field gradient, which could substantially reduce the current water treatment costs.

Sreeprasad et al.[120] performed an experiment on the adsorption of Hg(II) using two different rGO composites: rGO-MnO_2 and rGO-Ag. The adsorption experiments were conducted in batch modes at initial metal ion concentration 1 mg/L and temperature 303 ±2 K for both composites. The maximum adsorption capacities recorded were almost similar for rGO-MnO_2 and rGO-Ag, which were 9.50 and 9.53 mg/g, respectively.

An experiment to synthesize Fe_2O_4-rGO composites with different magnetic concentrations to remove As(III) and As(V) from water was performed by Chandra et al.[121] Similar experimental conditions of initial metal ion concentration 3.7 mg/L, pH 7.0, temperature 293 K, and contact time 2 hrs were applied for both ions. The values of adsorption capacity for the two ions were different, with As(V) having the higher capacity (13.10 mg/g) as compared to As(III) (10.20 mg/g). The adsorption kinetic studies could be described well by pseudo-second-order kinetic model. Furthermore, the isotherm data revealed that both ions followed the Langmuir isotherm model.

Chandra and Kim[122] have conducted an experiment to determine the ability of polypyrrole-rGO (Ppy-rGO) composite in removing Hg(II) from aqueous solutions. The maximum Hg(II) adsorption capacity was 980 mg/g at pH 3.0, temperature 298 K, contact time 3 hrs, and initial

concentrations 50 - 250 mg/L. Both Langmuir and Freundlich isotherm models prevailed in the isotherm study, as well as the pseudo-second-order kinetic model.

For the convenience of our readers, reported results for heavy metals removal from aqueous solution and wastewater on graphene based adsorbents were summarized in **(**Table 2).

4.2. Dyes adsorption on graphene and its derivatives

Alike heavy metals, abundant reported have been appeared for dyes adsorption on graphene and its derivatives. The following section will deal them in detail.

4.2.1. Adsorption on graphene and its composites

Liu et al.[23] studied the equilibrium and the dynamic adsorption of methylene blue (MB) from its aqueous solution onto graphene. The batch experiments showed that the adsorption of MB on graphene was dependent on adsorbent dosage, contact time and temperature. The optimum adsorption capacity of dyes increases from 153.85 to 204.08 mg/g with increase in temperature from 293to 333K, whereas the maximum percentage removal (99.68%) was observed at pH 10. The equilibrium data followed Langmuir isotherm model better than the Freundlich model. The adsorption kinetic of MB onto graphene fitted well to pseudo-second order model. Furthermore, the thermodynamic parameter revealed that the adsorption of MB onto graphene was an endothermic and spontaneous process.

An experiment was carried out by Li et al.[92] to investigate the adsorption of cationic red X-GRL from solution graphene. The adsorption properties of the cationic X-GRL onto graphene were studied as a function of pH, adsorbent dosage, contact time and temperature. The adsorption process was conducted at an initial concentration of 20-140 mg/L, contact time of 24 hrs and at temperatures of 288, 313 and 333K respectively. Therefore, the optimum adsorption capacity of 238.10 mg/g was obtained at 333K. On the other hand, the kinetic data was best described by

pseudo-second–order rate expression while the isotherm data matched the Langmuir model. The entire adsorption process was spontaneous and endothermic.

Wu et al.[123] performed an experiment an experiment to effectively removal methyl blue from aqueous solution by using graphene. The adsorption process was carried out at an initial concentration of 5 mg/L, temperature and contact time of 303K and 1 hr respectively. The thermodynamic analysis revealed a spontaneous and endothermic nature of the graphene due to π-π stacking interaction through fluoresce spectroscopy studies. The amount of dye adsorbed was found to be depended on the initial dye concentration.

The adsorption of organic dyes (RB, MB, fuchsine) in batch experiments on fabricated graphene–CNT hybrid aerogels (graphene/c-MWCNTs and graphene/ MWCNTs) by CO_2 drying of their hydrogen precursor was obtained from heating the aqueous mixture of GO and CNTs with ascorbic acid (vitamin C) without stirring Sui et al.[88] The adsorption process was conducted at room temperature with an initial dye concentration of 20 mg/L. The maximum adsorption capacities for RB, MB, and fuchsine by graphene/c-MWCNTs were 150.2, 191.2 and 180.8 mg/g, respectively, and 146.0, 134.9 and 123.9 mg/g, respectively, on graphene/MWCTs. Higher concentration of oxygen-containing functionalities in graphene/c-MWCNTs over graphene/c-MWCNTs might be a possible reason behind it.

An investigation was conducted by Zhao et al.[20] on a new graphene material known as "graphene sponges" (GSs) to adsorb both cationic (Methylene blue, Rhodamine B) and anionic (Methyl orange) dyes from their aqueous solution in a batch adsorption mode. The adsorption was conducted at constant temperature and initial concentration of 298K and 2×10^{-4} mol/L respectively. The contact of the two dyes differs with the cationic and anionic dye having a contact time of 4 to 24 hr, respectively. The maximum adsorption capacities of 184, 11.5 and 72.5 mg/g were obtained

for MB, MO and Rhodamine B respectively. Furthermore, from their experiment showed that basic dye (MB) has the highest adsorption capacity than the acidic dye (methyl orange) this may be due to the surface characteristic of the GSs and also due to the presence of the ionic charges on the dye. In addition, their studies also revealed that Rhodamine B can easily be desorbed from GSs in methanol or ethanol which suggests repeatable use of GSs from removing Rhodamine B from water.

The synthesis of magnetic Fe_3O_4-graphene composite (FGC) and its application in (MB, and Congo red (CR)) dyes removal from aqueous media was studied by Yao et al.[124] The maximum adsorption capacity - 33.66 mg/g was obtained at the temperature of 298±0.52K for CR, while the maximum adsorption capacity of 45.27mg/g was obtained at the temperature of 298±0.52K for MB. The equilibrium adsorption process was well fitted to Langmuir isotherm models for both MB and CR. Moreover, the kinetic data of MB and CR adsorption FGC was satisfied by a pseudo-second-order kinetic model.

Ai et al.[125] illustrated a facile one-step solvothermal method for the synthesis of graphene nanosheet (GNS)/magnetic (Fe_3O_4) composite and used for the removal of MB from aqueous solution. They studied the adsorption kinetics, isotherm, and thermodynamics in detail and their results revealed that the kinetic and equilibrium adsorption are well described by pseudo-second-order kinetic and Langmuir isotherm model, respectively. The observed maximum adsorption capacity at temperature - 298 K and initial concentration - 10-25 mg/L was 43.82 mg/g.

Furthermore, Graphene/magnetite composite was tested for the removal of pararosaniline (Basic Red 9) Wu et al.[126] The adsorption capacity - 198.23 mg/g was obtained at temperature - 298K, initial concentration - 20-60 mg/L and pH - 6.6±0.2. In this experiment, the value of pH played an important role on the adsorption performance, as increase in pH would precipitate the

dye. The adsorption kinetic followed the pseudo-second-order model while the adsorption isotherm was well interpreted by both Langmuir and Freundlich Isotherm model.

Wang and coworkers have synthesized magnetic sulfonic graphene nano-composite (G-SO_3H/Fe_3O_4) and used it as an adsorbent for the batch adsorption of three cationic (neural red, safrainin T, and victoria blue) and three anionic (methyl orange, brilliant yellow, and alizarin red) dyes from aqueous solution Wang et al.[93] The adsorbent G-SO_3H/Fe_3O_4 showed an excellent adsorption capacity toward the cationic dyes compared to anionic dyes. Based on their results, adsorption capacities of the three cationic dyes i.e. neural red, victoria blue and safrainin T were 216.8 mg/g, 20.06 mg/g and 199.3 mg/g, respectively, at initial concentration 20 – 250 mg/L, pH - 6, and room temperature. The adsorption of cationic dyes on G-SO_3H/Fe_3O_4 followed Langmuir isotherm and pseudo-second-order kinetics model. The adsorption capacity was found to follow decreasing order as neural red > victoria blue > safrainin.

In another development, graphene-sand composite (GSC) was prepared using asphalt as the carbon source and was used as an adsorbent for the removal of rhodamine 6G Sreeprasad et al.[127] The observed adsorption capacity was 75.4 mg/g obtained at a contact time 6hr and temperature 303 ± 2K. The adsorption kinetics data correlated well with pseudo-second-order kinetics model. It was also concluded that the importance of particle size of adsorbent cannot be over emphasized as it strongly dependent to the batch adsorption studies. Sen Gupta et al.[128] also tested the adsorption capability of graphene-sand composite (GSC) as an adsorbent for the removal of rhodamine 6G. It was found that the observed maximum adsorption capacity for rhodamine 6G under experimental conditions: initial concentration 5 mg/L, temperature - 303±2K and contact time - 8 hr was 55mg/g. The kinetics data obeyed pseudo-second-order kinetics model. Further, a column studies was also conducted and the break through curve at different bed depths were obtained. The bed depth service

time (BDST) model revealed an excellent agreement with dynamic flow experimental data. Finally, they were able to show that GSC can be regenerated using acetone for multiple uses.

An illustration on the capacity of graphene-carbon nanotube hybrid (G-CNT) to efficiently adsorb MB from aqueous solution was reported by Ai and Jian.[129] The initial dye ion concentrations tested were 10 – 30 mg/L, and the maximum adsorption capacity recorded for a contact time - 3 hr was 81.97 mg/g. Li et al.[130] synthesized Cu_2O-graphene and $Mg(OH)_2$-graphene Li et al.[131] and the adsorption of dyes, MB and RB was studied. Both composites exhibited an excellent behavior for dye removal.

4.2.2. Adsorption on GO and its composites

Other than graphene, the ability of GO as an adsorbent for the removal of dyes from aqueous medium was also investigated. The adsorptive potential of GO for MB from was tested by Yang et al.[132] The process was carried out under the following experimental condition: pH – 6, temperature – 298K, contact time – 1hr and initial dye concentration range – 0.188-1000g/L. It was illustrated that the amounts of MB adsorbed onto GO increased with an increase in pH and ionic strength while the removal process is faster and more effective at lower temperature. The highest removal efficiency of 99% and the maximum adsorption capacity of 714 mg/g were obtained. Moreover, the equilibrium data supported Freundlich isotherm. Finally, the result demonstrated that GO can be applied in the treatment of initial effluent and contaminated natural water.

A fast and effective adsorption of MB dye from an aqueous solution onto GO was reported by Zhang et al.[133] The dye containing solution had an initial concentration ranged between 0.33 and 3.3 mg/L, temperature – 298K, pH – 7.0 and contact time – 2hr. The maximum adsorption capacity was 1.939 mg/g. The adsorption processes became possible due to the special nano-structural properties and negatively change surface of GO and the positively charged MB ions which can be

easily absorbed electrostatically. The equilibrium adsorption data showed an excellent fit to Langmuir isotherm model and the adsorption process was exothermic in nature. The adsorption was found to be more efficient at high pH value and low temperature.

An experiment to determine the feasibility of removing methyl green dye from aqueous solution by using synthesized graphene nano-composite sheets was reported by Farghali et al.[134] At an initial concentration of 50-400 mg/L, the maximum adsorption capacities of methyl green onto the graphene sheets were found to be 203.51, 258.39 and 312.80 mg/g at temperature 298, 313 and 323K, respectively. The research showed that with increasing the concentration of methyl green in the solution, the active sites on graphene sheets are surrounded by many more methyl green ions, and the adsorption process would be carry out sufficiently. The study revealed better fitting of pseudo-second-order model to adsorption kinetics data. From the equilibrium adsorption data, the process was best fitted to the Langmuir isotherm data. An endothermic spontaneous and physisorption process was revealed from the thermodynamic study. Li et al.[135] prepared magnetic $CoFe_3O_4$ – functionalized graphene sheets ($CoFe_3O_4$- FGS) nano composite via a facile hydrothermal method and used it to adsorb methyl orange. The observed maximum adsorption capacity at 10 mg/L initial concentration was 71.54 mg/g. Pseudo-second-order model was best fitted to kinetics data.

Ramesh et al.[78] conducted an experiment to determine the capability of GO in adsorbing methylene blue, methyl violet, rhodamine B and orange G from aqueous solutions. Experiment revealed that GO has an excellent bonding affinity for cationic dye (i.e. methylene blue, methyl violet and rhodamine B). The research was performed at an initial concentration of 10-50 mg/L for both methylene blue and methyl violet at constant pH of 6 but varied the initial concentration of rhodamine B from 1-10 mg/L at pH 10 for methylene blue. The obtained adsorption capacities for methylene blue, methyl violent and rhodamine B were 17.3, 2.47 and 1.24 mg/g, respectively.

Large negative charge density available in aqueous solutions supported the effective adsorption of the cationic dye. Such adsorption behavior was contributed to the fact that methylene blue and methyl violet were positively charge whereas rhodamine B has both negative and positive charges associated with it existing between rhodamine B and GO. The kinetic data revealed that the dye followed the pseudo-second-order kinetic while the equilibrium data fitted well with the Langmuir.

The adsorption of MB from aqueous solution onto GO was reported under the following experimental conditions: temperature 298K, pH 6.0, initial dye concentration 40-120 mg/L and contact time 5 hr Li et al.[81] Results showed remarkable MB adsorption (243.90 mg/g) on GO. Moreover, the adsorption appeared to follow the Langmuir isotherm model, this revealed that the adsorption of MB on GO takes place in a mono layer adsorption manner. It is important to note that the change in the optimum MB adsorption capacity values may be because of the different experimental conditions employed during each study. The adsorption kinetics followed the pseudo-second-order mechanism, suggesting the adsorption might be a rate limiting step, involving valence forces through sharing or exchange of electrons between the adsorbent and adsorbate.

Sun et al.[136] had done a research on the use of modified GO for removing acridine orange from its aqueous solution. The efficiency of GO as an adsorbent was attempted to be enhanced through in situ reduction with sodium hydrosulfide ($Na_2S_2O_4$) since it is less toxic, less corrosion, and extremely eco-friendly. The laterally adsorption test was performed under similar experimental conditions of initial concentration 0.1 g/L, contact time 3hr and at a room temperature. The experiment was conducted with both pristine GO and in situ rGO. Experiment revealed that the in situ rGO had a much higher adsorption capacity (3333 mg/g) than the pristine GO (1428mg/g). Also, Sharma et al.[137] examined the possibility of using GO as an adsorbent for the removal of methyl green from aqueous medium at temperature 298 K and contact time 1 hr varying pH from 4 to 9, the adsorption capacities tend to increase from 4.821 to 7.613 mmol/g. The Langmuir isotherm

model and pseudo-second-order kinetic equation both governed the equilibrium and kinetic data, respectively.

Farahari et al.[138] had studied the adsorption mechanism of single and binary system of dye (Basic blue 41 (BB41), basic red 18 (BR18)) and basic red (BR46) by GO. The adsorption equilibrium showed that Langmuir Isotherm governed the experiment well, while showing a monolayer adsorption mechanism. The BB41, BR18 and BR46 adsorption capacities on GO were 1429, 1250, and 476 mg/g, respectively, and at a contact time of 1 hr, initial concentration of 5 mg/L and temperature of 298K. The adsorption kinetic followed the pseudo-second-order kinetic model, indicating, chemical adsorption process. In addition, the experiment revealed that dye removal with adsorbent dosage can be attributed to the increased adsorbent surface and availability of more adsorption site accessible for dyes molecules.

A series of GO with different oxidation degree was prepared using Hummer method and the fundamental behavior of the GO series for the removal of MB from aqueous solution was investigated and reported by Yan et al.[139] The MB containing in the solutions had an initial concentration – 600 mg/dm^3, pH – 7, temperature – 298K, and contact time – 0.25 hr. At varied degree of oxidation of GO_1, GO_2, GO_3, GO_4, GO_5 and GO_6, the maximum adsorption capacities of 40.6, 157.6, 334.7, 454.5, 513.9 and 570.4 mg/g, respectively, were achieved. The GO series exhibits stronger affinity to MB in water, resulting in fast dye removal rate and the pH independence with of adsorption capacity. It was concluded that by increasing oxidation degree, the dye uptake of GO are exponentially increased and the isotherm adsorption behavior would change from Freundlich to Langmuir type of adsorption. Finally, it can be deduced that the binding feature of MB loaded GO gradually change from MB molecule parallel stacking on graphite plane through

hydrophobic π – π interaction to vertical standing via electrostatic interaction with increase OD, resulting in a significant improvement of MB uptakes.

Li et al.[81] studied the adsorption of MB onto GO. From the experimental results, it was reported that the maximum adsorption capacity was 243.90 mg/g at room temperature under the experimental conditions: pH - 6.0, contact time - 5 hr, temperature - 297K and initial concentration of 100 mg/L. The isotherm study revealed that the equilibrium data followed the Langmuir isotherm model. The results also revealed that the adsorption of MB by GO adsorbent takes place in a monolayer adsorption manner. The adsorption kinetics followed the pseudo-second-order mechanism, suggesting the adsorption might be a rate limiting step, involving valence forces through sharing or exchange of electrons between the adsorbent and adsorbate.

The removal of cationic dyes, methyl blue (MB) and malachite green (MG) from aqueous solution using electrostatic attraction mechanism between dyes and GO was reported by Bradder et al.[140] The optimum adsorption capacities for MB and MG on GO were 351 and 248 mg/g, respectively, which were considerably higher than that of graphite and AC.

Zhang et al. [141] had done a research on the use of GO caged in cellulose bead (GOCB) for removing malachite green (MG) from aqueous solution. The lateral adsorption test was carried out under experimental conditions of pH - 7.0, contact time - 1hr, temperature - 298K and initial dye concentration - 10 mg/L. Under optimum conditions, the adsorption capacity was calculated to be 30.091 mg/g which was well fitted to the Langmuir isotherm model. The study also revealed that solution pH plays a very important role in the adsorption process as when the pH ranges from 6.0 to 8.0; this would increase the electrostatic attraction between the adsorbent and MG. Furthermore, when the pH was under 6 or above 8, the reason of it may be lie in the fact that GOCB decomposes in acidic solution and dissolved in alkaline condition.

The use of synthesis 3D graphene oxide sponge (GO Sponge) for the adsorption of cationic dyes, methylene blue (MB) and methyl violet (MV) was reported by Liu et al.[23] The 3D-GO sponge illustrates the adsorption capacities of 397 and 467 mg/g for MB and MV, respectively. The activation energies of the adsorption through the strong $\pi - \pi$ stacking and anion-cation interaction were 50.3 and 70.9 kJ/mol, respectively.

A covalent bonding technique to synthesize Fe_3O_4/SiO_2-GO nano-composite which also served as an adsorbent for the removal of MB from aqueous solution was reported by Yao et al.[142] The maximum MB adsorption capacities at temperatures 298, 318, and 333K were 97, 102.6 and 111.1 mg/g, respectively. The equilibrium data was well fitted to Langmuir isotherm model, while pseudo-second-order kinetics model was well fitted to kinetics data.

The possibility of using MgO ducked multi-layered graphene (MDMLG) for the removal of safrainin-O (SO) dye from water was reported by Rotte et al.[143] Maximum adsorption capacity of 3.92×10^{-4} mol/g was recorded under the following condition: pH -12, initial dye concentration - 4×10^{-4} M, contact time - 2hr. The adsorption increases with increase in pH and adsorbent dose. Removal% of SO dye decreases with increase in concentration. Isotherm and kinetics data fitted to Langmuir and pseudo-second-order model, respectively. Furthermore, the MDMLG showed an excellent reusability.

4.2.3. Adsorption on rGO and its composite

Kim et al.[144] reported the use of reduced rGO microstructure as an adsorbent for the removal of acid red 1 (AC1) and methylene blue (MB). The maximum adsorption capacity for MB was 302.11 mg/g which was achieved at initial concentration – 300 mg/L, while at initial concentration 50 mg/L, the maximum adsorption capacity for the AC1 was 28.51 mg/g. The equilibrium data for MB was fitted to Langmuir isotherm model, while Freundlich model was fitted to AC1. The adsorption

rates for both dyes are found to follow the pseudo-second-order kinetic. From the result it can be deduced that 3D rGO macrostructures were more favorable for the adsorption of cationic dye rather than the anionic dye due to strong specific interaction.

Sharma et al.[145] has conducted an experiment to study the adsorption of methyl green (MG) from aqueous solution using rGO. The experiment showed a remarkable adsorption capacity of 3.163 mmol/g at a set experimental condition: pH - 5, temperature - 298K, contact time - 1 hr. The equilibrium isotherm data was well described by, in the order of Toth>Skips>Dubinin-Radushkevich (D-R)>Scatchard>Langmuir>Temkin>Freudlich model at pH - 4-6. However, changes to D-R> Scatchard> Toth>Sips>Langmuir>Temkin>Freundlich model at pH 7-9. From the isotherm studies, Langmuir isotherm was best fitted to equilibrium data compared to Freundlich model. Furthermore, the experiment also revealed that pH of solution plays an important role in the adsorption process, increase in pH resulted to the increase in the adsorption capacity of MG onto rGO which was due to the effect of pH on electrostatic charge-charge interaction between the negatively charged polar groups to the cationic dye molecule. FTIR spectrum indicates that the adsorption was due to the electrostatic interaction between the MG and rGO nano-sheets. The kinetic data showed that the process was better described by pseudo-second-order kinetic model. Finally the negative ΔG^0 value of adsorption of MG onto rGO nano-sheet indicated that the process was spontaneous. While the value of ΔH^0, ΔS^0, activation energy values showed increase in adsorption capacity with temperature with physisorption process.

Three dimensional (3D) rGO-based hydrogels were synthesized by reduction of GO using sodium ascorbate and used as an adsorbent for the removal of MB and rhodamine B (RB) from aqueous solution Tiwari et al.[146] The experiments were conducted at an initial concentration – 0.5-10 mg/L, pH – 6.4, temperature – 298K and contact time – 2hr. The results revealed an excellent

removal capability of ~100% for MB and ~97% for RB when 0.6 g/L adsorbent dose was used. The maximum adsorption capacities for MB and RB were 7.85 and 29.44 mg/g, respectively. High adsorption capacity of RB was due to adsorption through strong $\pi - \pi$ stacking and anion–cation interactions. From the kinetic studies, it was revealed that the adsorption of dye followed the pseudo-second-order kinetics model. Furthermore, desorption studies were conducted using ethylene glycol showing that the rGO-based hydrogel could be efficiently regenerated and re-used. The results of the toxicity tests showed that hydrogel purified aqueous solutions were comparable to distilled water.

A one-pot solvothermal method was reported to successfully synthesize rGO supported ferrite (MFe_2O_4, M= Mn, Zn, Co and Ni) hybrids adsorbent for the removal of dye pollutants Bai et al.[147] After contact time of 2 min and initial dye concentration of 5 mg/L, 92% RB and 100% MB were effectively removed. Furthermore, the hybrid also showed an enhanced photo-catalytic activity for the degradation of RB and MB. Also, the possibility of using synthesized functional hybrid of rGO-Fe_3O_4 nano-particles was reported by Geng et al.[148] The hybrid possesses quite good and versatile adsorption capacity to different dye, RB, Rhodamine 6G (R6G), acid blue 92 (AB92), orange (II) (011), MG and new coccine.

An investigation was conducted by Nguyed-Phan et al.[149] on fabricated rGO-titanate (RGO-Ti) hybrids incorporating spherical TiO_2 nano particles with GO layers in the presence of NaOH for the removal of MB from aqueous solution. The optimum adsorption capacities was 83.26 mg/g at 10 mg/L initial concentration, which was higher than the adsorption capacity obtained for pure graphene (48.7 mg/g) and tubular titanates (36.5 mg/g). Wang et al.[150] performed an experiment to examine the removal of RB onto RGO/ZnO composite. The batch adsorption process was

conducted for contact time of 2 hrs, temperature - 298K and at initial dye concentration of 4-70 mg/L. The observed maximum adsorption capacity for RB was 32.6 mg/g.

A magnetic modified rGO (MrGO) nano-composite was prepared via one step solvothermal method Sun et al.[151] and was tested for its potential as an adsorbent to remove RB and MG dyes from aqueous solutions. The adsorption process was conducted at an initial concentration - 0.5-4 mg/L, contact time - 2hr, pH - 7.0 and temperature - 298K. The maximum adsorption capacities for RB and MG were 13.15 and 22.0 mg/g, respectively. The equilibrium data was well described by both Freundlich and Langmuir model, while kinetic study data fitted well to pseudo-second-order kinetic model. Desorption study using ethylene glycol as eluent revealed multiple rounds of recycle and reuse of MrGO without any significant change in initial adsorption efficiency. Wang et al.[152] pursued an experiment to study the adsorption of RB by core-shell structure polystyrene Fe_3O_4-GO nano-composites. The adsorption was carried out at an initial concentration of 0-150 mg/L, contact time of 24 hr and at room temperature. The maximum adsorption capacity was 13.8 mg/g.

The use of a synthesized super paramagnetic GO-Fe_3O_4 composite as a versatile adsorbent for the removal of MB and neutral red (NR) was reported by Xie et al.[153] The equilibration times for MB and NR were 30 min and 90 min with maximum adsorption capacity of 167.2 and 171.3 mg/g were obtained, respectively. The use of as-fabricated magnetic cyclodextrin/GO (MCGO) as an adsorbent from the removal of MB was demonstrated by Li et al.[154] This work depicted a maximum adsorption capacity 261.78 mg/g for MB, which was achieved at pH - 10, initial concentration - 100 mg/L, temperature - 303K and at a contact time - 5min. The experimental isotherm data followed Langmuir isotherm model, while the adsorption kinetic data obeyed the pseudo-second-order model. It was explained that the synergic effect of surface properties of GO, hydrophobicity of cyclodextrin and magnetic properties of Fe_3O_4 in MCGO composite provided a

versatile adsorbent with good adsorption properties and can be separable through magnetic separation after accomplishment of adsorption process.

Chen et al.[111] performed an experiment to effectively remove basic dye (MB) and acidic dye (eosin Y) from aqueous solutions by using GO-chitosan hydrogen composite. The adsorption process was conducted at initial concentration 0.8 mg/L, temperature 294±1K; however, the pH value and contact time were varied. For MB adsorption, pH - 6.5 at a contact time - 58 hr were set, while for eosin Y (acid dye), pH - 7.0 and a contact time - 36 hr were selected. Spectral method was used to determine the adsorption mechanism of dyes. Electrostatic interaction was found to be a major interaction that existed between the ionic dyes and hydrogen. In another study, Fan et al.[155] developed a magnetic chitosan-GO (MCFO) nano-composite through a covalent bonding of chitosan on the surface of Fe_3O_4 nano-particle followed by covalent functionalization of GO with magnetic chitosan. From their research, maximum methyl blue adsorption at an initial concentration - 60-200 mg/L, pH - 5.3, and temperature - 303K was 95.31 mg/g. Pseudo-second-order and Langmuir isotherm models were fitted to kinetics and isotherm data, respectively. The thermodynamic parameter data offered spontaneous and exothermic nature of the adsorption process. Desorption was maximum with 0.5M NaOH and the adsorption capacity was about 90% of the initial saturated adsorption capacity after four adsorption–desorption cycles.

The use of magnetic chitosan/GO composite (MCGO) as a versatile adsorbent for the removal of MB from aqueous solution was reported by Fan et al.[156] The maximum adsorption capacity at an initial concentration - 50-100 mg/L and temperature - 303±0.2K was 180.83 mg/g. The experiment proved that MCGO has an extraordinary adsorption capacity and fast removal rate for MB. Furthermore, an illustration on the capacity of magnetic β−cyclodextrin-chitosan GO nano-composite to adsorb MB from aqueous solution was done by Fan et al.[112] The amount of MB

adsorbed onto the magnetic β-cyclodextrin-chitosan/GO increased with dose. The adsorption of MB was governed by pseudo-second-order kinetics model. The isotherm data was well described by the Langmuir isotherm model with a maximum mono-layer adsorption capacity - 84.32 mg/g at temperature - 293K.

In a study carried out by Chen et al.[157] a hydrophilic and biocompatible three-dimensional (3D) chitosan-graphene meso-structure was prepared for the removal of reactive black 5(RB5) from aqueous solution. From their experiment it was revealed that at an initial RB5 concentration of 1.0 mg/mL, the RB5 removal efficiency was 97.5%. Also, the adsorption properties of Congo red (CR) onto graphene oxide (GO)/Chitosan (CS)/Etched (ETCH) were reported by Du et al.[158] The observed maximum adsorption capacity at pH - 3.0, initial concentration - 80 mg/L, and temperature - 283K was 294.12 mg/g. The experimental isotherm data pursued Langmuir isotherm model, while the adsorption kinetics data fitted well with the pseudo-first-order model. From their experimental result, it can be deduced that GO/CS/ETCH was a promising adsorbent candidate to remove dyes from wastewater.

The use of 3D graphene oxide-sodium alginate (GO-SA) gel and reduced graphene oxide-sodium alginate (rGO-SA) gel as an adsorbent for the removal of MB was investigated and reported by Ma et al.[159] Maximum MB adsorption capacity on GO–SA and rGO-SA at an initial concentration - 0.1mmol/L, temperature - 303K and contact time - 12 hr was found to be 833.3 and 192.3 mg/g, respectively. The equilibrium data fitted well with both Langmuir and Freundlich isotherm, while pseudo-second-order model and the intra particle diffusion model well described the kinetic data. Thermodynamic parameters indicated that the adsorption of MB was a spontaneous process. Moreover, the type of oxygen containing groups in both GO-SA and rGO-SA gels can result to different adsorption mechanism. Electrostatic interaction play a leading role between GO-

SA and MB, while π – π stacking was the primary interaction between rGO-SA and MB. In addition to that, the adsorption of GO-SA was exothermic, while the absorption of rGO-SA was an endothermic.

Yu et al.[109] performed an experiment to determine the adsorption capacities of GO-Zeolite and carboxy-GO/Zeolite powder in the removal of RB from aqueous solution. The maximum adsorption capacity values of RB on GO-Zeolite and carboxy-GO/Zeolite were 55.56 and 67.56 mg/g, respectively. The adsorption behavior was fitted to Langmuir isotherm while kinetics data was fitted to pseudo-second-order kinetics model. Li et al.[81] on the other hand, conducted a study to evaluate the adsorption possibility of GO/calcium alginate (GO/CA) composite as an adsorbent for the removal of MB from aqueous solution. The adsorption studies were conducted under the following experimental condition: initial concentration - 30-80 mg/L, pH - 4.5-10.2. Temperature played a very important role in the adsorption process. Decrease in adsorption capacity from 163.93 to 140.85 mg/g with increase in temperature from 298 to 328 K was observed signifying the exothermic nature of the process. In addition, maximum adsorption capacity (181.81 mg/g) was reported at 0.05g/100mL. Kinetics data obeyed pseudo-second-order model, while equilibrium data fitted to Langmuir isotherm model.

Deng et al.[160] conducted an experiment on the use synthesized magnetic GO (MGO) as adsorbent for the removal of ionic dyes including MB and orange G (OG) from aqueous solution. They conducted their experiment at constant experimental condition of contact time 6.75 hr and temperature 298K, regardless; the values of adsorption capacity for the two dyes were different at different concentration with MB having higher capacity (64.23 mg/g) at 90 mg/L of its initial concentration, as compared to OG (20.85 mg/g) at an initial concentration of 60 mg/L. Furthermore, they give a detail explanation on the adsorption of MB and OG onto MGO by electrostatic

attraction mechanism between MGO surface charge adsorbents; because of the electrostatic attraction force; MGO adsorbent with negative charge surface at higher pH (>3.5) favored the adsorption toward the cationic dye MB with positive charge. In contrast, for anionic dye OG, The adsorption quality decreased with increasing pH value due to electrostatic repulsion force. The adsorption isotherm data of the dyes were fitted well with Langmuir model in mono-component system, while the adsorption kinetic study followed the pseudo-second-order model.

The use of fabricated polydopamine layer coated GO (PD/GO) composite for the removal of MB was reported by Dong et al.[161] The maximum adsorption capacity of MB by different percentage of PD i.e. PD5%/GO, PD15%/GO, PD35%/GO and PD70%/GO were 1.3, 1.89, 1.7 and 0.6 g/g, respectively. From the equilibrium isotherm study, the data fitted well with the Langmuir model showing monolayer MB coverage over adsorbent surface. Moreover, it was showed that the superior adsorption capacity of the sub-nano thick PD layer coated GO made it a promising adsorbent for decontaminating wastewater. Table 3 summarized the reported results for dye removal from aqueous solution and wastewater on graphene based adsorbents.

5. Graphene as adsorbent – Major challenges

The science of graphene as adsorption material is growing rapidly, however, there are many challenges and hurdles need to be manipulated. Though, the raw materials required for graphene synthesis are naturally abundant, but still it is a challenge for graphene scientist to modify and/or to develop methods resulting to come up with the adsorbents which are highly selective and have high adsorption potential. The graphene-based materials with low aggregation and high specific surface areas show high adsorption capacity for organic pollutants especially benzene-containing compounds, where $\pi - \pi$ interaction between graphene and adsorbate plays a dominant role. [19, 162,

[163, 164] Therefore, one of the major problems faced in using graphene as an adsorbent is the aggregation of graphene sheet, it is important to prevent this aggregation between the layers; this is because the aggregations tend to limits the available adsorption site bonding accessibility with pollutants. The aggregation can be avoided by the introduction of oxygen groups that will served as a powerful approach. Moreover, those oxygen groups improved the dispersion properties of graphene in the solutions which can greatly increase the removal ability of graphene. In another development for convenient separation, magnetic particles are introduced in the adsorbent to form magnetic graphene composite. The added magnetic particles will also play an important role in preventing aggregation of the graphene.

The present technique for the synthesis of graphene on large scale is the Hummer's method which involves oxidation and reduction process. Some of the major drawbacks of this method are that the oxidation process consumes large quantity of strong acids and oxidants and produces large amount of acidic wastes which requires high cost for its treatment and safe disposal. Hence, it may be environment unfriendly and expensive method. Furthermore, hydrazine used in this method is a suspected carcinogen and hazardous to the environment. Strong oxidation process may give rise to unwanted defects in graphene, which will significantly compromise graphene superior properties. Hummer's method cannot produced graphene sheet with controlled size and desired geometrical shapes. Therefore, exploration of other methodologies to tackle the aforementioned issues is extremely urgent.

In order to tackle some of the aforementioned problems, scientists have put forward few solutions. Many different oxidation processes of graphene in the categories of chemical/thermal oxidation have been introduced and established for desired results. In addition, the use of the hydrazine can be avoided by substituting it with ascorbic acid (vitamin C) which is non-toxic and environmental friendly. The utilization of a milder exfoliation process with assistance of additional

species like multi-pyrene tethered amphiphiles. Lee et al.[77] may present the feature synthetic direction as it will produce graphene sheets with controllable size and internal conjugated structure.

Finally, it is well known that a single graphene sheet has a superior mechanical properties, however, mechanical properties of pure collective graphene products or graphene composites, are usually significantly compromised by the weak inter sheet interaction. Therefore, at present there remains a major challenge regarding how to strengthen the interaction between the adjacent graphene sheet or the interaction between the graphene sheet and it modifier functionalities. As graphene can be modified via either covalent or non-covalent binding e.g. $\pi - \pi$ stacking, hydrogen etc, multi- functional inter-graphene "welding" molecule or metallic nano-particles might be a good alternative to improve the inter-layer electrical communication.

Hence, the synthesis of GO and rGO is challenging as there is always a need to look into a more facile, robust and efficient preparation method of GO, graphene and their composites. Based on some other reports and in our own experience, it has been realized that the complete understanding of graphene structure still needed exhaustive studies and research practices owing to great chemistry that can be plausible from GO and graphene are rapidly expanding. Another important aspect that needs to be addressed is to look for better synthetic approaches which demonstrate better reproducible and controlled methods.

6. Conclusions and future research perspectives

In this review, applications of graphene and its derivative for heavy metals and dyes removal have been presented. The preparation of high quality graphene and its derivatives in a cost effective and ecofriendly manner on large scale is essential for many applications. In case of electrostatic interaction, anionic pollutants are usually favored by low pH value. Anions have been proposed to

adsorbed through specific and non-specific adsorption. Nevertheless, the adsorption of cations and anions is based on the three adsorption mechanisms such as electrostatic interaction, ion exchange and complex formation. The adsorption isotherm and kinetic can be described by Langmuir isotherm, and pseudo-second order model. The adsorption process for graphene-based materials is spontaneous, endothermic and feasible.

A comprehensive application of graphene nano-composites shows a great potential in dealing with organic and inorganic pollutants in the environment. Due to the outstanding physicochemical properties of graphene, it will play a very important role in environmental pollution management in the future. Firstly, in the detection of organic and inorganic pollutants, graphene nano-composite revealed its great potentiality in environmental application. However, it is still too early to implicate large scale application of these nano-composites in environmental monitoring and remediation due to the essential question that arises over both in short and long term exposure of graphene to the ecosystem and human being remain largely unaddressed. Despite of these challenges, graphene nano-composite, however are still one of the most exciting platforms for energy and environmental studies. Secondly, the preparation of graphene material via “chemical” processing routes (for example oxidation of graphene followed by reduction of the GO platelet obtained by exfoliation may be able to produce fairly large amount of “graphene” cost effective). However, the chemical details (for example oxidation/reduction mechanism and detail chemical structure) needed to be fathom. Very few graphene-based materials have been produced and analyzed, when compared to other well-known nano-materials; thus, it is recommended for future studies to evaluate the feasibility to produce more graphene-based materials, with further developments in the nano-material manufacturing.

Moreover, the revolutionary applications based on graphene and its composites with the advances in both fundamental physics and chemistry and practical techniques, will expand the horizons of graphene nano-composites and open-up new window in human life.

Acknowledgements

The authors would like to thank the Malaysia-Japan International Institute of Technology (MJIIT) for providing the grant to conduct this research. One of the authors (SAZ) is grateful for research funding from Kwangwoon University in 2015.

References

1. F. Fu, Q. J. *Env. Managt.,* 2011, **92,** 407–418.

2. F. Marahel, M. A. Khan, M. Ehsan, B. Iman, H. Soraya, *Desalination and Water Treatment,* 2015, **53,** 826-835.

3. N. M. Julkapli, S. Bagheri, S. B. Abd Hamid, *The Scientific World Journal,* 2014, 2014 Article ID **692307**, 25.

4. H. Hou, R. Zhou, P. Wu, L. Wu, *Chem. Eng. J.* 2012, 211–212: 336–342.

5. A. R. Karbassi, S. Nadjafpour, *Environ. Pollu.,* 1996, **93,**257–260.

6. M. Soylak, Y. E. Unsal, N. Kizil, A. Aydin, *Food Chem. Toxicol.,* 2010, **2,** 517–521.

7. E. Makrlik, P. Vanura, J. Radioanal. *Nucl. Chem.,* 2005, **267,** 233–235.

8. A. E. Ofomaja, E. B. Naidoo, S. J. Modise, *J. Environ. Manag.,* 2010; **91,** 1674–1685

9. M. M. Matlock, B. S. Howerton, D. A. Atwood, *Ind. Eng. Chem. Res.,* 2002, **41,** 1579–1582.

10. A. Dabrowski, Z. Hubicki, P. Podkos´cielny, E. Robens, *Chemosphere,* 2004, **56,** 91–106.

11. M. M. Rao, D. K. Ramana, K. Seshaiah, M. C Wang, S. W. C. Chien, *J. Hazard. Mater.,* 2009, **2**, 1006–1013.

12. J. R. C. Parga, D. L. Cocke, J. L.Valenzuela, J. A. Gomes, M. Kesmez, G. Irwin, H. Moreno, M. Weir, *J. Hazard. Mater.,* 2005, **124,** 247–254.

13. S. A. Nasier, *Chem. Biochem. Eng. Q.,* 2013, **17,** 219-224.

14. A. J. B. Dutra, A, Espinola, P. P. Borges, *Meneral Eng.,* 2000, **13,** 1139-1148.

15. G. Ayoub, L. Semerjian, A. Acra, M. Fadel, B. Koopman, *Bittern J. Envirn. Eng.,* 2001, **127,** 196-207.

16. M. Imamoglu, O. Tekir, *Desalination,* 2008, **228,** 108–113.

17. J. Xu, S. T. Yang, J. Lao, *Review in organic chemistry,* 2013, **33,** 139-169.

18. J. Zhu, S. Wei, H. Gu, S. B. Rapole, Q. Wang, Z. Luo, N. Haldolaarachchige, D. P. Young, Z. Guo, *Environ. Sci. Technol.,* 2012, **46,** 977-985.

19. G. L. J. Zhao, X. Ren, C. Chen, X. Wang, *Environ. Sci. & Techn.,* 2011, **45,** 10454-10462.

20. Zhao G. W. T. C. Chen, X. Wang, *RSC Advances,* 2012, **2,** 9286–9303.

21. L. W. Xiao, S. L. Yu, Y. L. Tang, *Progress in Chemistry,* 2013, **25,** 419–430.

22. Y. Len, W. Guo, S. Su, C. Yi, L. Xing, *Chem. Eng. J.,* 2012; 211-212.

23. L. L. C. Liu, C. Bao, Q. Jia, P, Xiao, X. Liu, Q. *Talanta,* 2012, **93,** 350-357.

24. F. Fang, L. Kong, J. Huang, S. Wu, K. Zhang, X. Wang, B. Sun, Z. Jin, J. Wang, X-J. Huang, J. Liu, *J. Hazard Mater.,* 2014; **270,** 1-10.

25. P. Gansan, R. S. Vasudevan, *J. Taiw. Inst. of Chem. Engr.,* 2013, **44,** 808-814.

26. C. Schafhäutl, U. d-V. d-Kohlenstoffes mit Silicium, Eisen, and anderen Metallen, welche die verschiedenen Gattungen von Roheisen, Stahl und Schmiedeeisen bilden*, J. Prakt. Chem.,* 1840, **21,** 129–157.

27. B. C. Brodie, *Trans. R. Soc. London*, 1859, **149,** 249.

28. L. Staudenmaier, Verfahren zur Darsatellung der Graphitsaure Ber. Dtsch. *Chem. Ges.,* 1898; **31,** 1481-1487.

29. H. P. Boehm, A. Clauss, Hofmann U, G. O. Fishcher, *Proceedings of the Fifth Conference of carbon,* 1962.

30. A. J. Van Bommel, J. E. Crombeen, A. Van Tooren, *Surface Sci.,* 1975, **48,** 463-472.

31. H. P. Boehm, R. Setton, E. Stumpp, *Carbon,* 1986, **24,** 241-245.

32. K. S. Novoselov, A. K. Geim, S. V. Morozov, D. Jiang, Y. Zhang, S. V. Dobonos, I. V. Griorieva, *Science,* 2004, **306,** 666-669.

33. M. D. Stroller, S. ark, Y. Zhu, R. S. Jinho, Ruoff. *Nano Lettes,* 2008, **8,** 3498–3502.

34. K. L. Bolotin, K. J. Sikes, Z. Jiang, M. Klima, G. Funderberg, J. Hones, P. Kim, H. L. Stormer, *Solid State Commum.,* 2008, **146,** 351–355.

35. S. Basu, P. Bhattacharyya, *Sen Actuators B: Chemical*, 2012, **173,** 1-21.

36. W. L. I. Choi, R Seelaboyina, Y. S. Kang, *Crit. Rev. Solid State Mater. Sci.,* 2010, **35,** 52-71.

37. C. Lee, X. Wei, J. W, Kysar, J. Hones, *Sci.,* 2008, **321,** 385-388.

38. A. A. Balandin, S. Ghosh, W. Bao, I. Calizo, D. Teweldebrhan, F. Miao, C. C. N. Lau, *Nano Letter,* 2008, **8,** 902–907.

39. L. Kui, Z. GuiXia, W. Xiangke, *Chinese Science Bullet*, 2012, **57,** 1223-1234.

40. Y. Zhu, S. Murali, W. Cai, X. Li, J. W. Suk, J. R. Potts, R.S. Ruoff, *Adv. Mater.,* 2010, **22,** 3906–3924.

41. A. K. Geim, K. S.Novosolov, *Natural Material*, 2007, **3,** 183-191.

42. W.S. Hummers, Jr, R. E. Offeman, J. *Am Chem. Soc.,* 1958, **80,** 1339-1339.

43. A. M. Dimiev, S. M. Bachilo, R. Saito, J. M. Tour, *ACS Nano,* 2012**, 6,** 7842–7849.

44. K. Loh. P. K. Bao, J. Ang, Yang. *J. Mater. Chem.,* 2010, **20,** 2277-2289.

45. M. J. McAllister, J. Li. D. H. Adamson, H. C. Schniepp, A. A. Abdala, J. Liu, M. H. Alonso, D. L, Milius, R. Car, R. K. Prud'homme, I. A. *Chem. Mater.,* 2007, **19,** 4396-4404.

46. C. Junghun, L. Hangil, K. Ki-jeong, K. Bongsoo, K. Sehun, *Phys. Chem. Lett.,* 2010,**1,** 505-509.

47. B.Claire, S. Zhirmin, L. Xuebin, W. Xiaosong, B. Nate, N. Cecil, M. Dddier, T. Li, H. T. Joanna, A. N, Marchenkov, H. Edward, P. N. Conrad, First, A. H. Walt, *Sci.,* 2006, **312,** 1191-1196.

48. W. A. C. de Heer, X. Wu, P. N. First, E. H. Conrad, X. Li, T. Li, M. Sprinkle, J. Hass, M. L. Sadowski, M. Potemski, G. Martinez, Pionic. *Solid State Comm.,* 2007, **143,** 92-100.

49. T. Seyller, A. Bostwick, K.V. Emtsev, K. Horn, L. Ley, J. L. McChesney, T. Ohta, J. D. Riley, E. Rotenberg, *Phys. Stat. Sol.,* 2008,**245,**1436-1446.

50. S. K. Y. Some, E. Hwang, H. Yoo, H. Lee, *Chem. Comm.,* 2012, **48,** 7732-7734.

51. L. Dan, G. Gordon, Wallace, B. Marc, S. Müller, G. Richard, B. Kaner, *Nature Nanotech*., 2008, **3,** 101 -105.

52. V. C. Tung, M. J. Allen, Y. Yang, R. B. Kaner, *Nature Nanotech*., 2009, **4,** 25-29.

53. C. Lahiri, Kang, S. *Critical Reviews in Solid State and Mater. Sci.,* 2010, **35,** 52-71.

54. K. Wang, J. Ruan, H. Song, J. Zhang, Y. Wo, S. Guo, Cui.. *Nanoscale. Res. Lett.,* 2010, DOI 10.1007/s11671–010–9751–6 (Epub ahead of print).

55. W. Zhang, C. Zhou, W, Zhou, A. Lei, Q. Zhang, Q. Wan, B. Zou, *Bull Environ. Contam. Toxicol.,* 2011, **87,** 86-90

56. M. C. Duch, G. R. Budinger, Y. T. Liang, S. Soberanes, D. Urich, S. E. Chiarella, L. A. Campochiaro, A. Gonzalez, N. S. Chandel, M. C. Hersam, G. M. Mutlu, *Nano Lett.,* 2011, **11,** 5201 – 5207.

57. A. Schinwald, F. A. Murphy, A. Jones, W. MacNee, K. Donaldson, *ACS nano.,* 2012, **6,**736-746.

58. A. C. Ferrari, J. C. Meyer, V. Scardaci, C. Casiraghi, M. Lazzeri, F. Mauri, S. Piscanec, D. Jiang, K. S. Novoselov, S. Roth, A. K. Geim, *Physical Review Letters,* 2006, **97,** 187401

59. C. Wang, L. Zhan, W. M. Qiano, L. C. ling, *New carbon meter*, 2011, **26,** 21

60. G. Titelman, V. Gelman, S. Bron, R. L. Khalfin, Y. Cohen, H. Bianco-Peled, *Carbon,* 2005, **43,** 641-649.

61. Y. M. Ren, N. Yan, Q. Wen, Z. J. Fan, T.Wei, M. L. Zhang, J. Ma, *Chem. Eng. J.,* 2011, **175,** 1–7.

62. J. I. Goldstein, D. E. Newbury, P. Echlin, D. C. Joy, A. Roming, C. E. Lyman, C. FIori, E. lifshin, New York. 1992.

63. Y. Hernande, V. Nicolosi, M. Lotya, F. M. Bligh, Z. Sun, S. De, I. T. McGovern, B. Holland, M. Byrne, Y. K. Gunko, J. J. Boland, P. Niraj, G. Duesberg, S. Krishnamurthy, R, Goodhue, J. Hutchison, V. Scardaci, A. C. Ferrari, J. N. Coleman, *Nat. Nanotechn.,* 2008, **3,** 563-568**.**

64. P. C Ma, J. K. Kim, B. Z. Tang, *Carbon*, 2006, **44,** 3232-3238.

65. D. Yang, A. Valamakanni, P. S. Bozoklu, M. Stoller, R. D. Piner, *Carbon,* 2009, **47,** 145-152.

66. D Li, M. R. Muller, R. B. Gilje Kaner, G. G. Wallace, *Nature Nanotech.,* 2008, **3,** 101-103.

67. S. Stankovich, D. A. Dikin, R. D. Piner, K. A. Kohlheaas, A. Kleinhammes, Y. Jia, Y. Wu, S. T. Nguyen, R. S. Ruoff. *Carbon*, 2007, **45,** 1558-1565.

68. J. Shen, Y. Hu, M. Shi X Lu, C. Qin, C Li, M. Ye, *Chem. Mater.*, 2009, **21,** 3514–3520.

69. M, Kaustubha, D. Dababrata, N. B. Manindra, *J. Sep. Purif. Tech.,* 2008, **58,** 311-319.

70. N. Zhang, H. Qiu, Y. Si, W. Wang, J. Gao*, Carbon,* 2011, **49,** 827–837.

71. A .A. Norizilah, Fakhrul-Razi, S.Y.C. Thomas, C. Luqman, *J. Nanomaterials,* 2011, ID 495676: 8.

72. Z. J. Fan, W. Kai, J. Y. Yan, T. W. Wei, L. J. Zhi, J. Feng, Y. M. Ren, L. P. Song, F. Wei, *ACS Nano,* 2011, **5,** 191–198.

73. W Wu, Y. Yang, H. Zhou, T.Ye, Z.Huang, R. Liu, Y. Kuang, *Water Air Soil Pollut.,* 2013, **224**,1372.

74. Y. Ren, N. Yan, J. Feng, J. Ma, Q. Wen, L. Nan, D. Qing, *Mat. Chem. and Phys.,* 2012, **136,** 538-544.

75. C. J. Madadrang, H. Y. Kim, G. Gao, N. Wang, J. Zhu, H. Fen, M. Gorrring, M. L. Kasner, S. Hou, *ACS Appl. Mater Interfaces,* 2012, **4,** 1186-1193.

76. S. Pei, H-M. Cheng, *Carbon,* 2012, **50**, 3210–3228.

77. D-W. Lee, T. Kim, M. Lee, *Chem. Commun.,* 2011, **47**, 8259-8261.

78. G. K. Ramesha, A. V. Kumara, H. B. Muralidhara, S. Sampath, *J. Colloid Interface Sci.,* 2011, **361**, 270-277.

79. A. Hu, A.Apblett, Lecture Notes in Nanoscale Science and Technology, ISBN: 978-3-319-06577-9, 2014,22.

80. D. Chen, L. Tang, J. Li, *Chem*. *Soc*. *Rev*., 2010, **39**, 3157–3180.

81. Y. Li, Q. Du, T. Liu, X. Peng, J. Wang, J. Sun, Y. Wang, S. Wu, Z. Wang, Y. Xia, L. Xia, *Chemical engineering research and design,* 2013, **91**, 361–368.

82. Y. Leng, W. Guo, S. Su, C. Yi, L Xing. *Chem. Eng. J.,* 2012, **212**, 406-411.

83. C-F. Chang, T. Q. Duc, J-R Chen, *App. Surf. Sci.,* 2013, **264**, 329-334.

84. Z-H. Huang, X. Zheng, W. Lv, M. Wang, Q-H. Yang, F. Kang, *Langmuir,* 2011, **27**, 7558–7562.

85. Y. Wu. H. Luo, H. Wang, C. Wang, J. Zhang, Z. Zhang, *J. of Colloid and Inter. Sc.,* 2013, **394**,183-191.

86. L. Hao, H. Song, L. Zhang, X. Wan, Y. Tang, Y. Lv, *J. of Colloid and Inter. Sc.,* 2012, **369**, 381-387.

87. X. Deng, L. Lu, H. Li, F. Luo. *J. Hazard. Mater.,* 2010, **183**, 923-930.

88. Z. Sui, Q. Meng, X. Zhang, R. Ma, B. Cao, *J. Mater. Chem.,* 2012, **22**, 8767-8771.

89. Y. Yuan, G. Zhang, Y. Li, G. Zhang, F. Zhang, X. Fan, *Polymer Chemistry,* 2013, **4**, 2164-2167.

90. H. Jabeen, V. Chandra, S. Jung, J. W. Lee, K. S. Kim, S. B. Kim, *Nanoscale*, 2011, **3**, 3583-3585.

91. D. Nandi, K. Gupta, A. K. Ghosh, A. De, S. Banerjee, U. C. Ghosh, *J. Nanopart. Res.,* 2012, **14**, 1272.

92. Z. J. Li, F. Chen, L.Y. Yuan, Y. L. Liu, Y. L. Zhao, Z. F. Chai, W. Q. Shi, *Chem. Eng. J.,* 2012, **210**,539-546.

93. H. Wang, X. Yuan, Y. Wu, H. Huang, G. Zeng, Y. Liu, X. Wang, N. Lin, Y. Qi, *Appl. Surf. Sc.,* 2013, **279**, 432-440.

94. R. Sitko, E. Turek, B. Zawisza, E. Malicka, E. Talik, J. Heimann, A. Gagor, B. Feist, R. Wrzali. *Dalton Trans,* 2013, **42**, 5682-5689.

95. Y-C. Lee, J-W. Yang*, Ind. Eng. Chem.,* 2012, **18**, 1178-1185.

96. Y.L. F. Musico, C. M. Santos, M. L. P. Dalida, D. F. Rodrigues, *J. Mater. Chem.,* 2013, **1**, 3789-3796.

97. X. Mi, G. Huang, W. Xie, W. Wang, Y. Liu, J. Gao, *Carbon,* 2012, **50**, 4856−4864.

98. H. Cheng, K. Zeng, J. Yu, *Journal of Radio analytical and Nuclear Chemistry,* 2013, **298**, 599-603.

99. S. Luo, X. Xu, G. Zhou, C. Liu, Y. Tang, Y. Liu, J. *Hazard Mater.,* 2014, **274,**145-155.

100. Y. Lei, Y. Luo, L. Zhang, *Chemical Physics Letters*, 2014, **593**, 122-127.

101. X. Yuan, Y. Wang, J. Wang, C. Zhou, Q. Tang, Rao X. *Chem. Eng. J.,* 2013, **221**, 204-213.

102. X-J. Hu, Y-g. Liu, H. Wang, A-w. G-m. Chen, Zeng, S. Liu, Y. Guo, X. Hu, T. Li, Y. Wang, L. Zhou, S. Liu, *Sep. and Purif. Tech.,* 2013, **108**,189-195.

103. X. Luo, C. Wang, L.Wang, F. Deng, S. Luo, X Tu, C. Au, *Chem. Eng. J.,* 2013, **220,** 98-106.

104. K. Zhang, V. Dwivedi, C. Chi, J. Wu, *J. Hazard. Mater.,* 2010, **182**, 162-168.

105. M Liu, C. Chen, J. Hu, X. Wu, X. Wang, *J. Phys. Chem. C.,* 2011, **115**, 25234-25240

106. S. Li, X. Lu, Y. Xue, J. Lei, T. Zheng, C. Wang. *PLoS One,* 2012, 7:e43328.

107. F. Peng, T. Luo, L. Qiu, Y. Yuan. *Materials Research Bulletin*, 2013, **48**, 2180–2185.

108. P Zong, S. Wang, Y. Zhao, H. Wang, H. Pan, C. He. *Chem. Eng. J.,* 2013, **220**, 45-52.

109. B. Yu, J. Xu, J-H. Liu, S-T. Yang, J. Luo, Q. Zhou, J. Wan, R. Liao, H. Wang, Y. Liu, *J. of Env. Chem. Eng.,* 2013, **1**, 1044-1050.

110. Y. Q. He, N. N. Zhan, X. D. Wang, *Chin Chemical Letter,* 2011, **22**, 859-862

111. Y. Chen, L. Chen, H. Bai, L. Li, *J. Mat. Chem. A.,* 2013, **1**, 1992-2001.

112. L. Fan, C. Luo, S. Min, L. Xiangjuan, Q. Huamin, *Colloids and Surfaces B: Biointerfaces,* 2013, **103,** 523-529.

113. L. Li, S. L. Fan, M. Sun, H. Qiu, X. Li, H. Duan, C. Luo. *Colloids and Surfaces B: Biointerfaces*, 2013, **107**, 76-83.

114. W. M. Algothmi, N. M. Babdaru, Y. Yu, J. G. Shapter, A. V. Ellis, *J. Colloid and Interf. Sci.,* 2013, **397**, 32-38.

115. S. Yang, L. Li, Z. Pei, C. Li, X. Shan, B. Wen, S. Zhang, L. Zheng, J. Zhang, Y. Xie, R. Huang, *Carbon,* 2014, **75**, 227-235.

116. R. Li, L. Liu, Yang F. *Chem. Eng. J.,* 2013, **229**, 460-468.

117. P. Bhunia, G. Kim, C. Baik, H. Lee, *Chem. Commun.,* 2012, **48**, 9888-9890.

118. C. Wang, H. Luo, Z. Zhang, Y. Wu, J. Zhang, S. Chen, *J. Hazard. Mater.,* 2014; 268:124-131.

119. Y. Zhang, L. Yan, W. Xu, X Guo, L. Cui, L. Gao, Q. Wei, B. Du, *J. Mol. Liq.,* 2014, **191**, 177-182.

120. T. S. Sreeprasad, S. M. Maliyekkal, K. P. Lisha, T. *J. Hazard. Mater.,* 2011, **18**, 921-931.

121. V. Chandra, J. Park, Y. Chun, J. W, Lee, I. C Hwang, *ACS Nano,* 2010, **4**, 3979-3986.

122. C. Chandra, K. S. Kim, *Chem. Commun.,* 2011, **47**, 3942–3944.

123 T. C. X. Wu, S. Tan, H. Li, J. Liu, W. *Chem. Eng. J.,* 2011, **173**, 144-149.

124. Y. Yao, S. Miao, S. Liu, L-P. Ma, H. Sun, S. Wang, *Chem. Eng. J.,* 2012, **184**, 332.

125. L. Ai, C. Zhang, Z. Chen. J. *Hazard. Mater.,* 2011, **192**, 1515-1524.

126. Q. Wu, C. Feng, C. Wang, Z. Wang, *Colloids and Surfaces B: Biointerfaces***,** 2013, **101**, 210 214.

127. T. S. Sreeprasad, Sen, S. Gupta, S. M. Maliyekkal, T. Pradeep. *J. Hazard. Mater.,* 2013, **246–247**, 213-220.

128. S. Sen Gupta, T. S. Sreeprasad, S. M. Maliyekkal, S. K. Das, T. Pradeep. *ACS Appl. Mater. Interfaces,* 2012, **4**, 4156-4163.

129. L. Ai, J. Jiang, *Chem. Eng. J.,* 2012, **192**, 156-163.

130. B. Li, H. Cao, G. Yin, *J. Mater, Chem.,* 2011, **21**, 10645-10648.

131. B. C. H. Li, G. Yin, *J. Mater. Chem.,* 2011, **21**, 13765-13768.

132. S.-T. Yang, S. Chen, Y. Chang, A. Cao, Y. Liu, H. Wang, *J. Colloid Interface Sci.,* 2011, **359**, 24-29.

133. W. Zhang, C. Zhou, W. Zhou, A. Lei, Q. Zhang, Q. Wan, B. Zou, *Bull. Environ. Contam. Toxicol.,* 2011, **87,** 86-90

134. A. A. Farghali, M. Bahgat, W. M. A. El-Rouby, M. H. Kherdr, *Journal of Alloys and Compounds,* 2013, **555**, 193-200.

135. N. Li, M. Zheng, X. Chang, G. Ji, H. Lu, L. Xue, P. Lija, C. Jieming, *J. Solid State Chem.,* 2011, **184**, 953-958.

136. L. Sun, H. B. Yu, *J. Hazard Mater.,* 2012, **203–204**, 101-110.

137. P. Sharma, M. R. Das. J. *Chem. Eng. Data,* 2013, 58, **1**, 151–158.

138. H. Z. Farahani, H. H. Monfared, N. M. Mohmoodi, *Desalination and Water Treatment*, 2014, Doi:10.1080/19443994.2014.960462, 1-13.

139. H. Yan, X. Tao, Z. Yang, K. Li, H. Yang, A Li, R. Cheng, *J. Hazard Mater.,* 2014, **268**, 191-198.

140. P. Bradder, S. K. Ling, S. Wang, Liu, *J. Chem. Eng. Data,* 2011**, 56**, 138-141.

141. X. Zhang, H. Yu, H. Yang, Y. Wan, H. Hu, Z. Zhai, *J. Colloid Interface Sci.,* 2015, **437**, 277-282.

142. S.-T., Yang, S. Chen, Y. Chang, A. Cao, Y. Liu, H. Wang, *J. Colloid Interface Sci.,* 2011, **359**, 24-29.

143. N. R. Rotte, S. Yerramala, J. Bonoface, V. V. S. Srikanth, *Chem. Eng. J.,* 2014, **258**, 412-419.

144. H. Kim, S-O. Kang, S. Park, S. H. Park, *J. Ind. and Eng. Chem.,* 2014, JIEC-**2060**, 6.

145. P.Sharma, B. K. Saikia, M. R. Das, *Colloids and Surfaces A: Physicochemical and Engineering Aspects,* 2014, **457**, 125-133.

146. J. N. Tiwari, Mahesh, K. N. H. Le, K. C Kemp, R. Timilsina, R. N. Tiwari, K. S. Kim, *Carbon*, 2013, **56**, 173-182.

147. S. Bai, Z. X. Shen, Y. Liu, G. Zhu, X. Xu, K Chen, *Carbon,* 2012, **50**, 2337-2346.

148. Z. Geng, Y. Lin, X. Yu, Q. Shen, L. Ma, Z. Li, N. Pan, X. Wang, *J. Mater. Chem.,* 2012, **22**, 3527-3535.

149. T.-D. Nguyen-Phan, V. H. Pham, E. J. Kim, E-S. Oh, S. H. Hur, J. S. Chung, B. Lee, E. W. Shin, *Appl. Surf Sci.,* 2012, **258**, 4551-4557.

150. J. T. T. Wang, B. Tang, X. Hou, L. Sun, X. Wang, *ACS Appl. Mater. Interfaces,* 2012, **4**, 3084-3090.

151. H. C. L. Sun, L. Lu, *Nano Res,* 2011, **4**, 550-562.

152. J. Wang, B. Tang, T. Tsuzuki, Q. Liu, X. Hou, L. Sun, *Chem. Eng. J.,* 2012, **204/206**, 258-263.

153. G. Xie, P. Xi, F. Liu, L. Huang, Y. Shi, F. Hou, Z. Zeng, C. Shao, J. Wang, *J. Mater, Chem.,* 2012, **22**,1033-1039.

154. L. Li, L. Fan, H. Duan, X. Wang, C. Luo, *RSC Adv.,* 2014, **4**, 37114-37121.

155. L. Fan, C. Luo, X. Li, F. Lu, H. Qiu, M. Sun, *J. Hazard. Mater.,* 2012, **272279,**215–216.

156. L. Fan, C. Luo, M. Sun, X. Li, F. Lu, H. Qiu, *Bioresour. Technol.,* 2012, **114**, 703-706.

157. Z. X. Chen, Z. M. Zhao, Y. L. Cao, X. P Ai, H. X. Yang, J. Liu. *Adv. Energy Mater.,* 2011, **2**, 95–102.

158. Q. Du, J. Sun, Y. Li, X. Yang, X. Wang, Z. Wang, L. Xia, *Chem. Eng. J.,* 2014, **245**, 99-106.

159. T. Ma, P. R. Chang, P. Zheng, F. Zhao, X. Ma, *Chem. Eng. J.,* 2014, **240**, 595-600.

160. J-H. Deng, X-R. Zhang, G-M. Zeng, J-L. Gong, Q-Y. Niu, J. Liang, *Chem. Eng. J.,* 2013, **226**,189-200.

161. Z. W. D Dong, X. Liu, X. Pei, L. Chen, J. Jin, *J. Mater. Chem. A.,* 2014, **2**, 5034-5040.

162. S. B. Yang, J. Hu, C. L. Chen, D. Shao, X. Wang, *Environ. Sci. Tech.,* 2011, **45**, 3621-3627.

163. D. D. Shao, Z. Q. Jiang, X. Wang, *Chemosphere,* 2011, **82**, 751-758.

164. D. D. Shao, G. D. Sheng, C. L. Chen. *Chemosphere,* 2010, **79**, 79-685.

165. A. C. G. A. Neto, N. M. R. Peres, *Physical world,* 2006, **19**, 33-37.

166. M. I. Katsnelson, Zitterbewegung, *Eur. Phys.,* 2006, **51**,157-160.

167. A. Bianco, Angew, *Chem. Int. Ed.,* 2013, **52,** 4986-4997.

168. G. Zhao, X. Ren, X. Gao, X. Tan, J. Li, C. Chen, Y. Huang, X. Wang, *Dalton Trans.,* 2011, **40,** 10945.

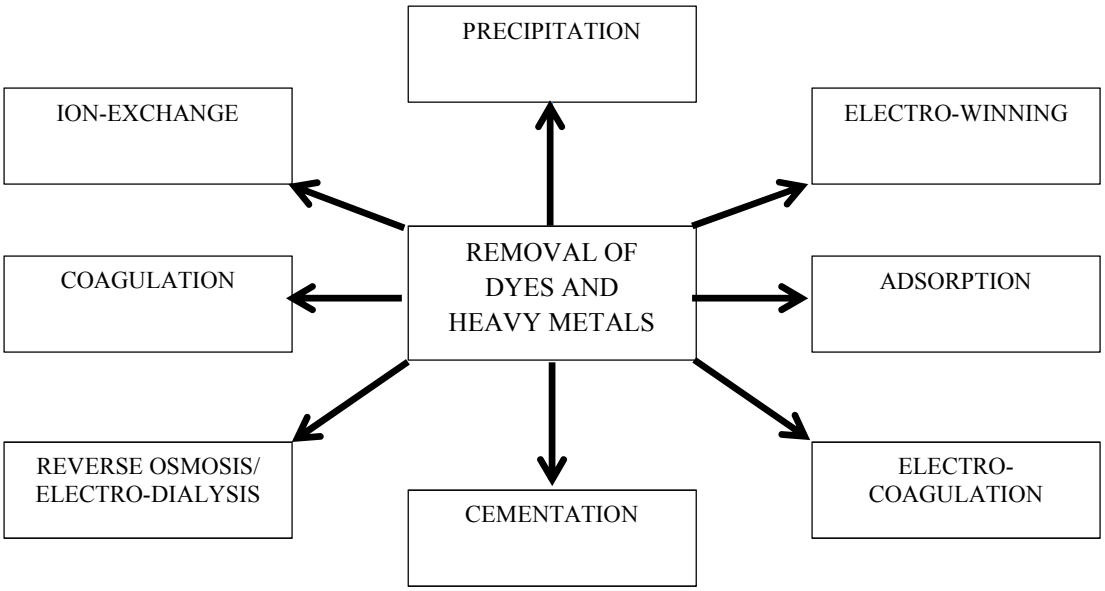

Fig. 1 Conventional methods for the removal of dyes and heavy metal ions.

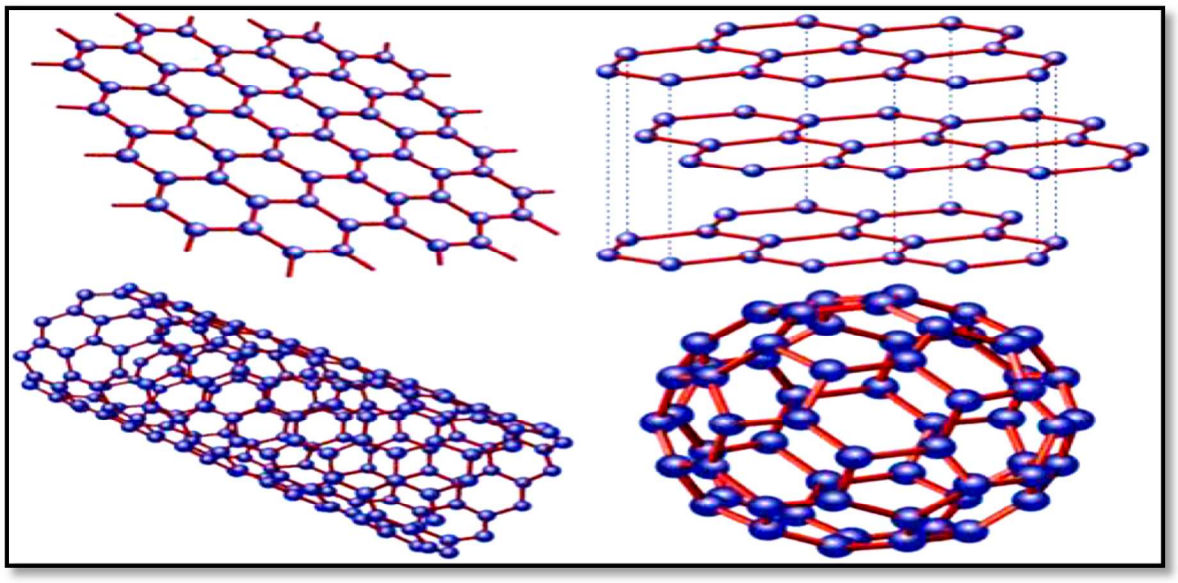

Fig. 2 Graphene (Top left) is a honeycomb lattice of carbon atoms. Graphite (Top right) can be viewed as a stack of graphene Layer. Carbon nanotubes are rolled-up cylinders of graphene (Bottom left). Fullerenes (C60) are molecules containing of wrapper graphene through the introduction of pentagon on the hexagonal lattice.[165]

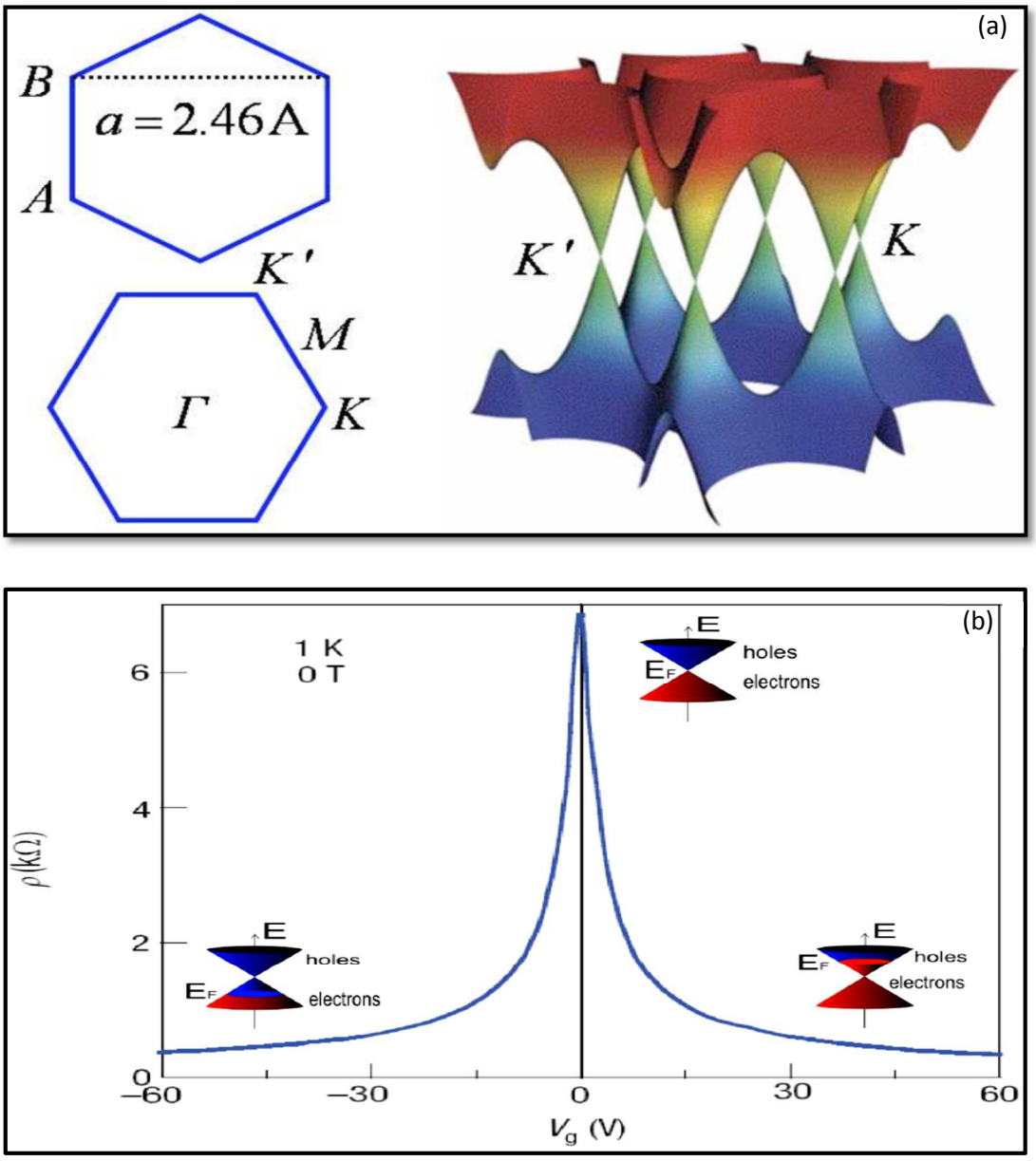

Fig. 3 Band structure of graphene at low energies. The conduction and valence bands intersect at points K and K/. The dispersion relation is linear at that point **(a).**[166] Ambipolar electric field effects in monolayer graphene. The inset cones represent low-energy spectrum E(k), indicating changes in the position of the Fermi energy (EF) with increasing (inducing electron) or decreasing (inducing holes) gate voltage (Vg). The rapid decrease in resistivity ρ by adding charge carriers describes their high mobility and does not noticeably change up to room temperature **(b).**[41]

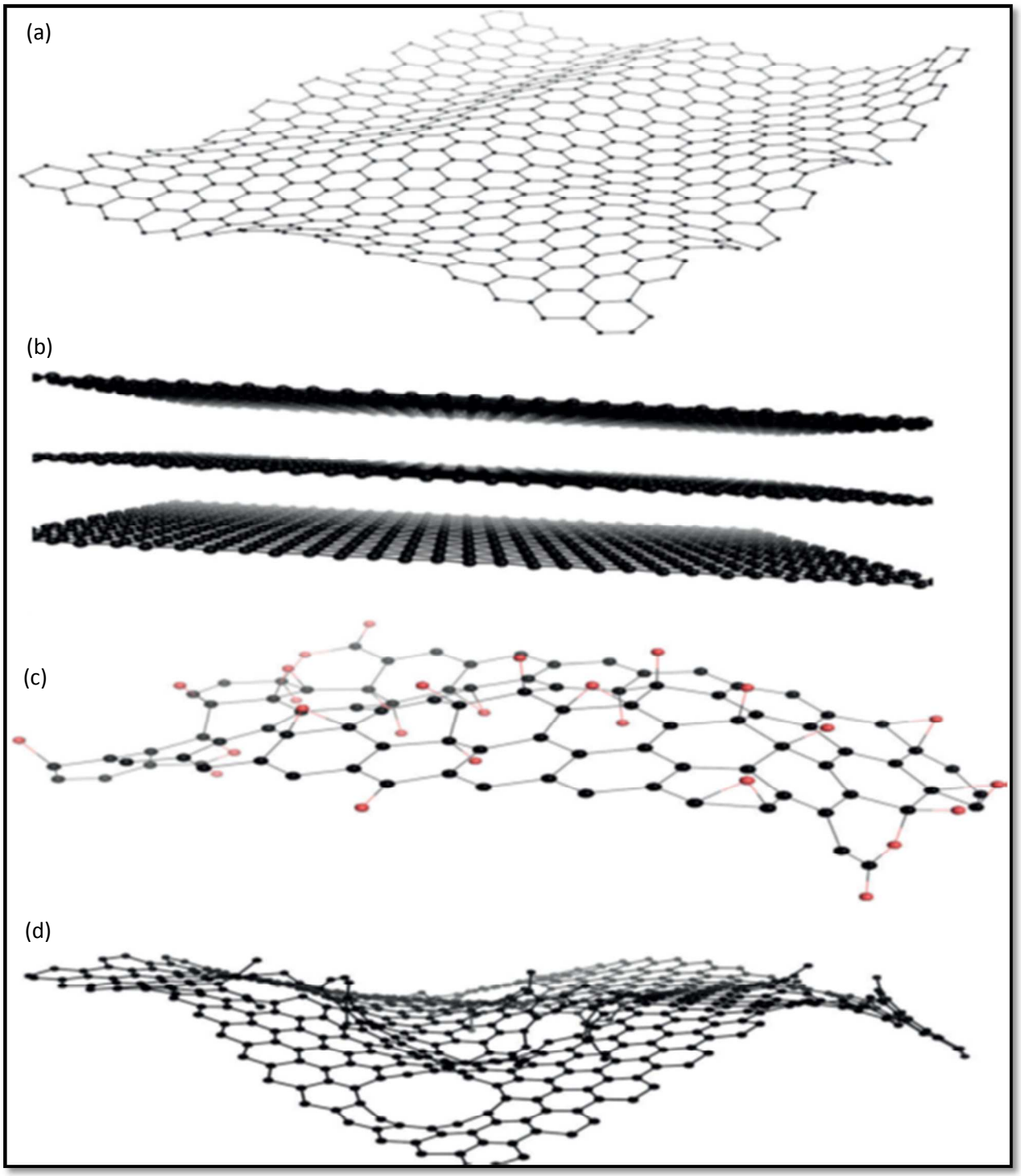

Fig. 4 Representative chemical structures of some of the members of GFNs: graphene (a), few-layer graphene (b), graphene oxide (oxygen atoms are in red) (c), and reduced graphene oxide (d) [167]

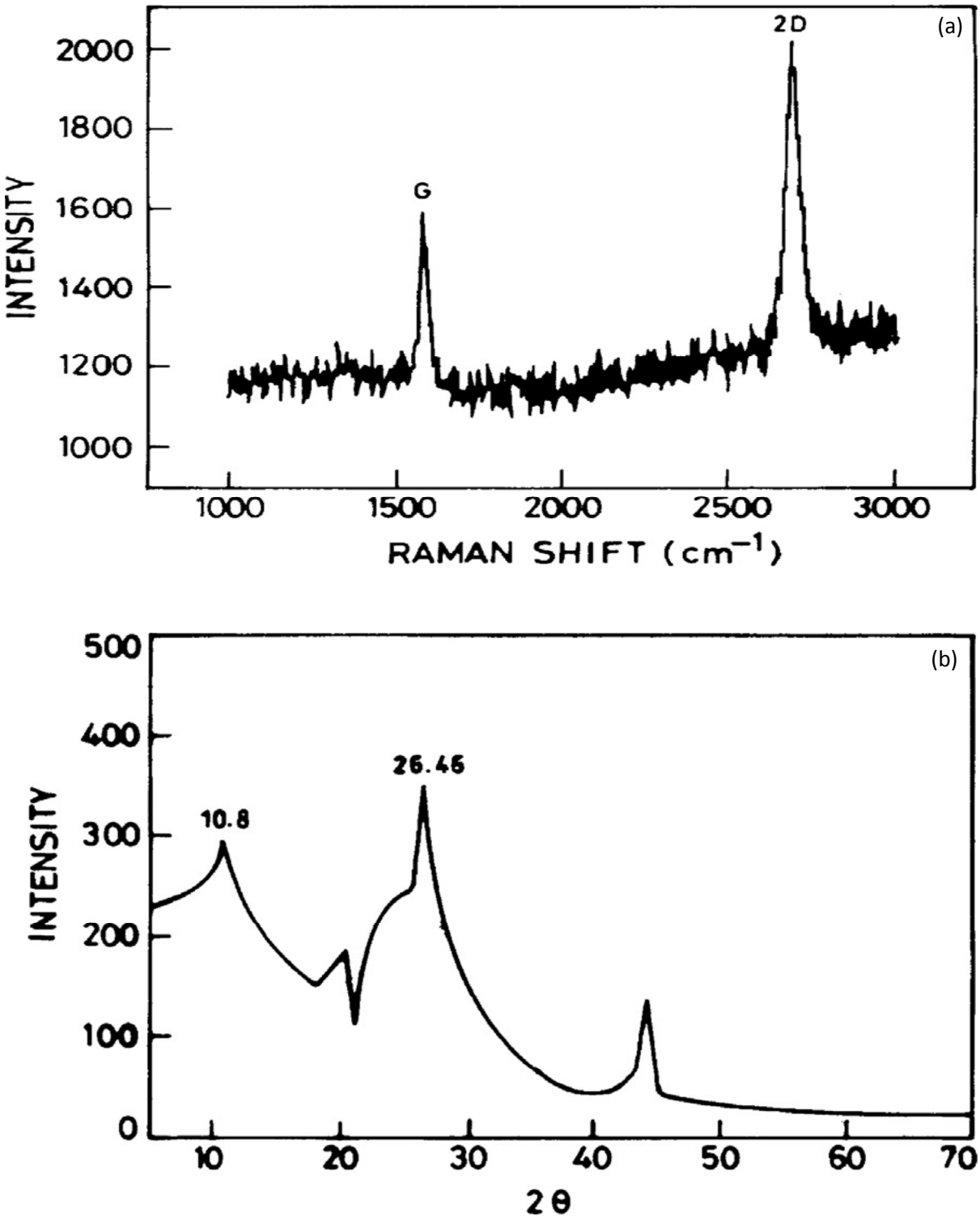

Fig. 5 Typical Raman spectra **(a),** [23] and XRD patterns[25] of graphene

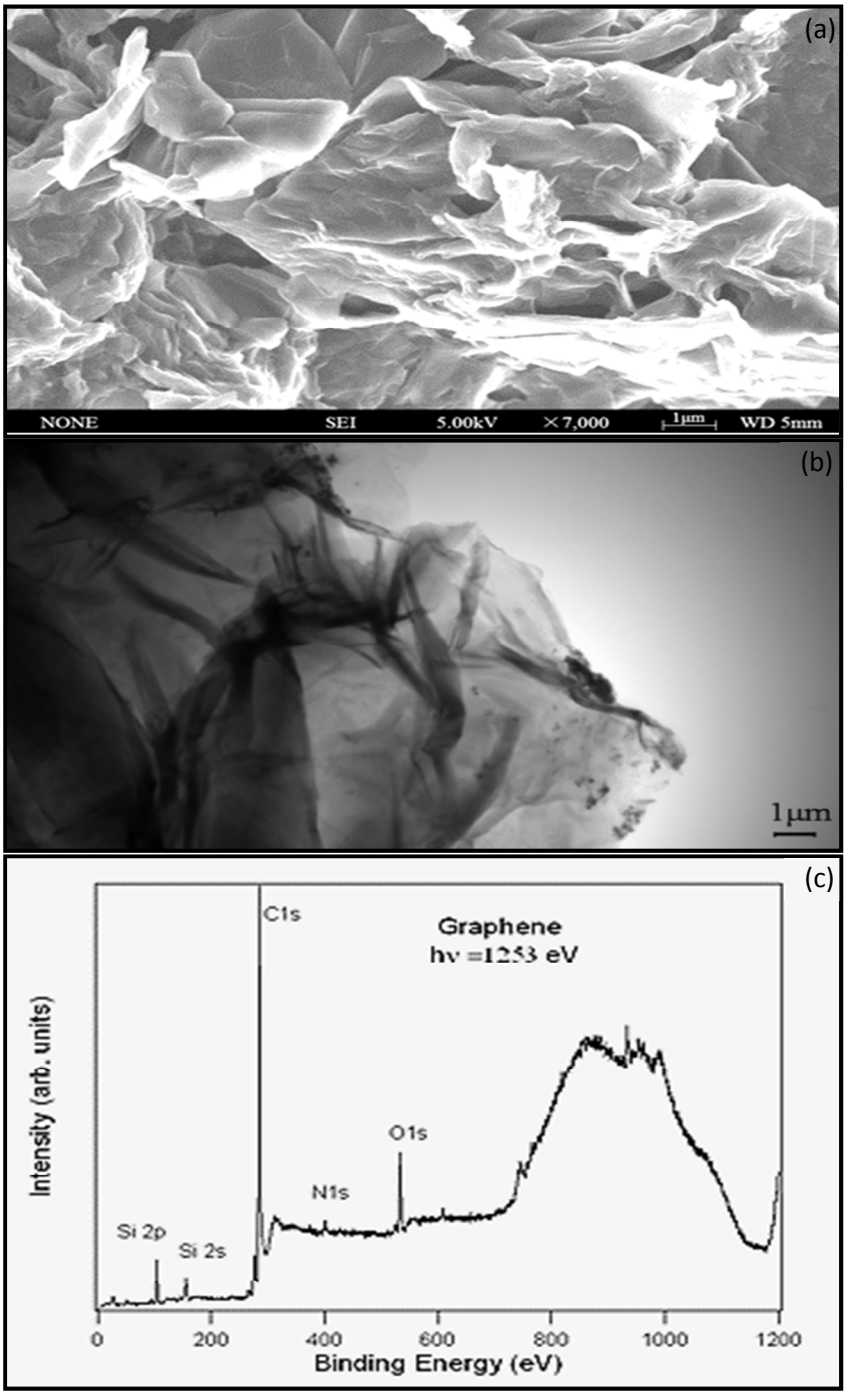

Fig. 6 SEM image **(a),** [85] TEM image **(b),** [85] and wide XPS scan of cleaved UITAR **(c)** [25] of graphene.

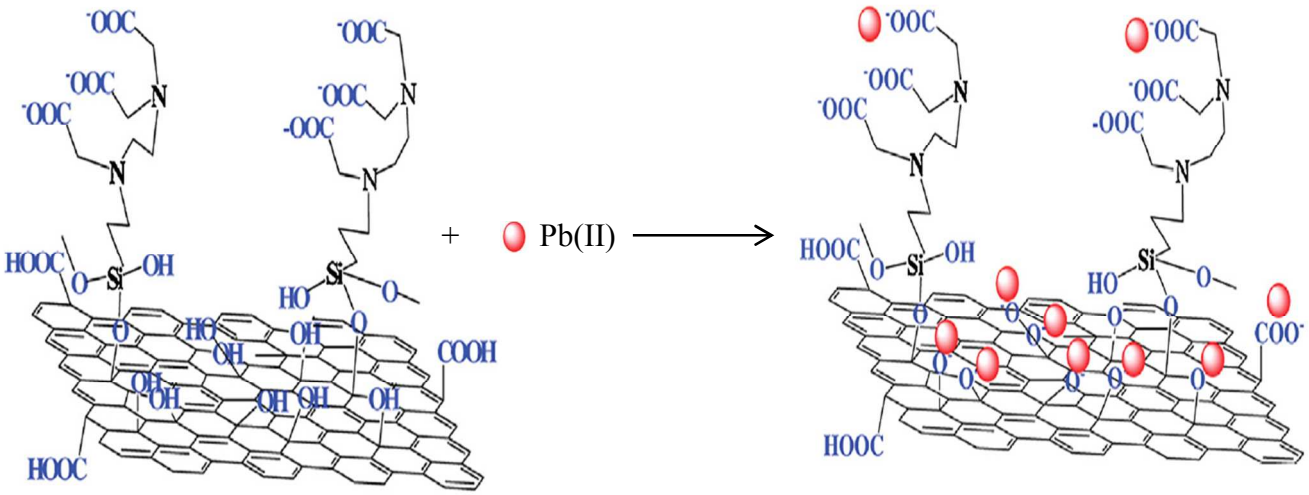

Fig. 7 EDTA modified GO and its interaction with bivalent heavy metal ion.[75]

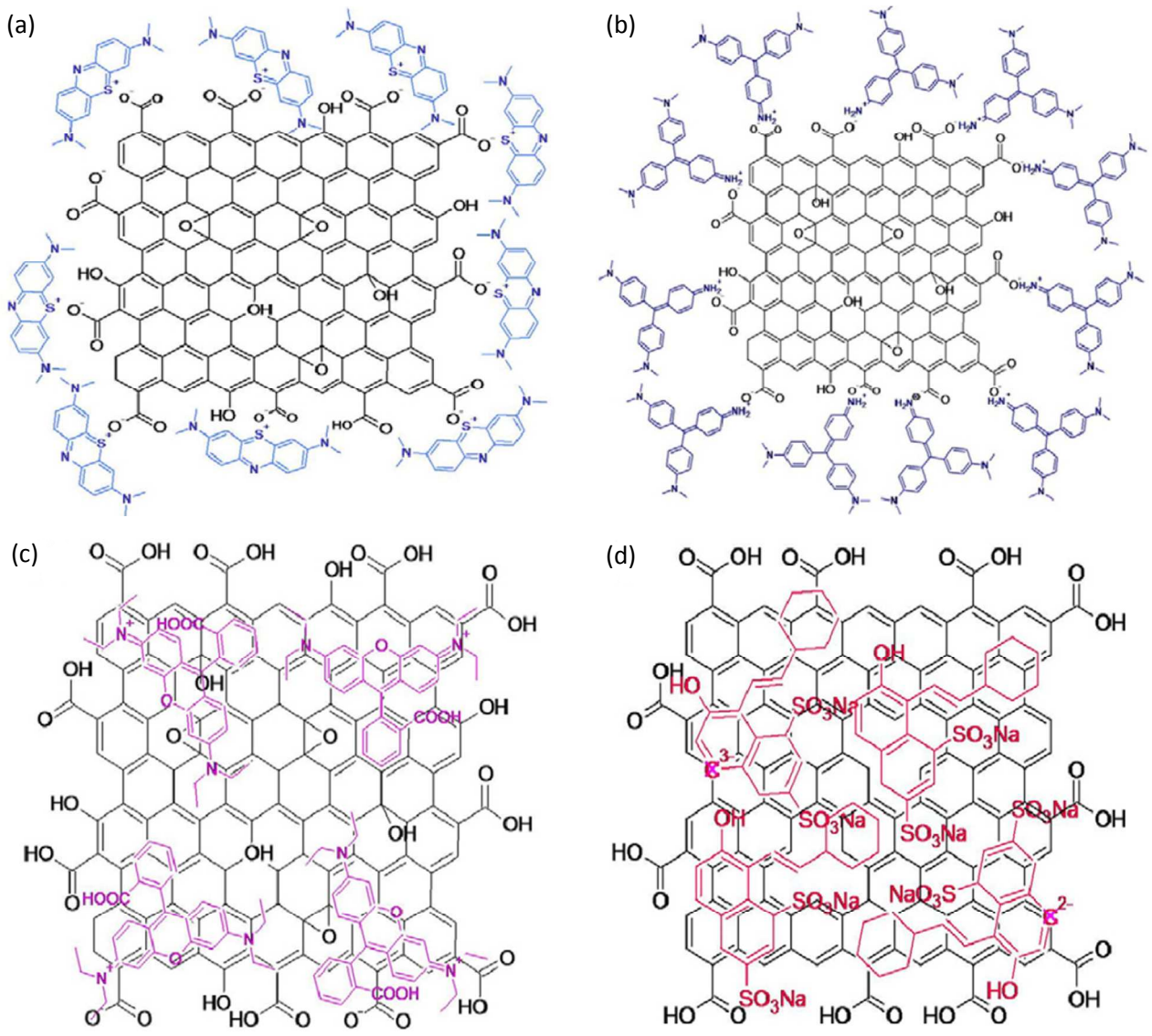

Fig. 8 Schematic interactions of EGO/MB **(a)**, EGO/MV **(b)**, EGO/RB **(c)**, and rGO/OG **(d)**.[78]

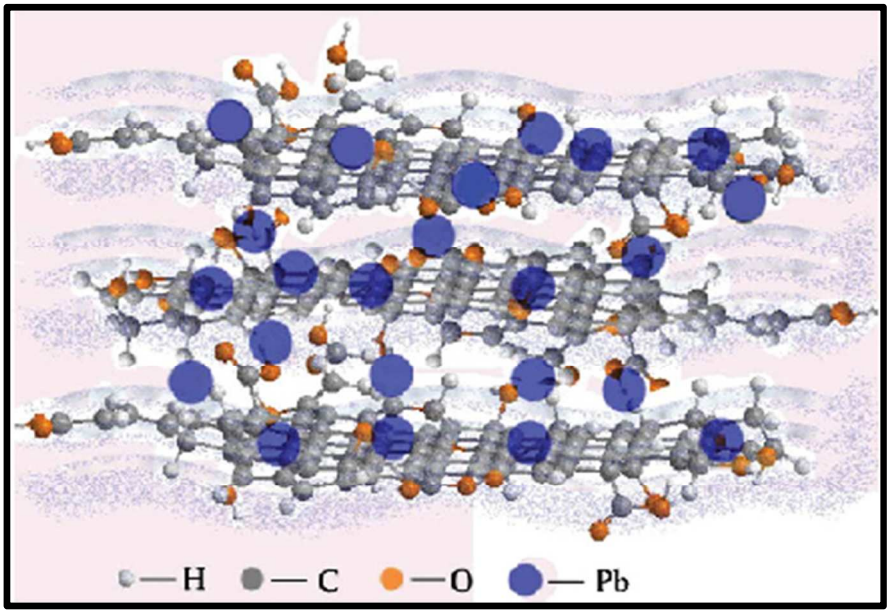

Fig. 9 Illustration showing the adsorption mechanism of heavy metal ions on graphene.[168]

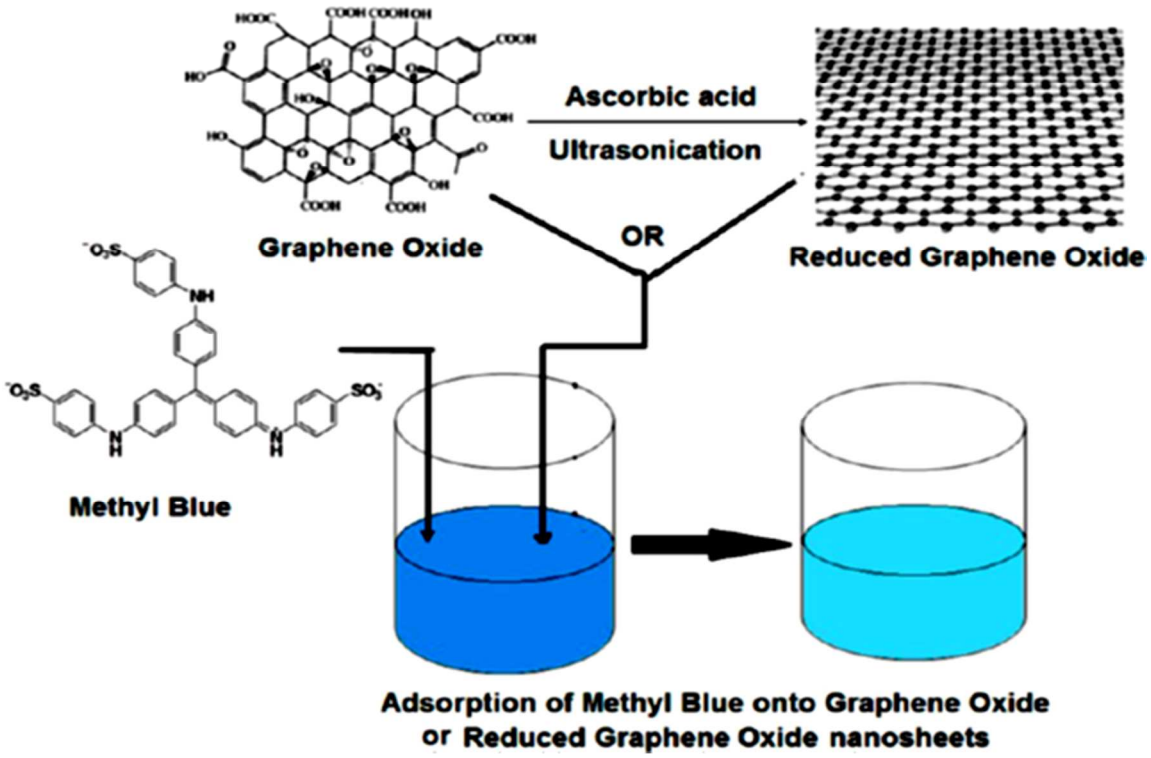

Fig. 10 Schematic diagram of adsorption mechanism of dyes onto GO or rGO nanosheets.[137]

Table 1. Graphene synthesis methodologies

Methodology	Merits	Demerits
Micromechanical Exfoliation	• High quality properties	• Low Yield • Not scalable
Epitaxial Sic Growth	• Large continuous film area	• Not transferable • High Temperature • Low vacuum
Reduction of GO	• Solution Processed • High yield	• Poor electrical properties • Small area flakes
CVD	• High quality • Large area • Transferable	• High temperature • Low vacuum • Difficult Scalability
Solution Exfoliation	• High quality • Good Scalability • Low temperature	• Small area graphene flasks • Colloidal stability

Table 2. Summary of reported results for heavy metals removal from aqueous solution and wastewater by graphene based adsorbents

Adsorbent	Adsorbate	Adsorption Capacity	Conc.	pH	Temp. (K)	Contact time (h)	Models applicable		Reference
							Isotherm	Kinetic	
Graphene	Pb(II)	22.42 mg/g	40 mg/L	4.0	303	15	Langmuir		84
Graphene (treated at 77 K)	Pb(II)	35.21 mg/g	40 mg/L	4.0	303	15	Langmuir		84
Graphene (treated at 973 K)	Pb(II)	35.46 mg/g	40 mg/L	4.0	303	15	Langmuir		84
Graphene	Sb(II)	10.92 mg/g	1-10 mg/L	11.0	303	4	Freundlich	Pseudo-second-order	82
Graphene	Fe(II)	299.3 mg/g	20 mg/L	8.0		24			83
Graphene	Co(II)	370 mg/g	20 mg/L	8.0		24			83
Graphene	NO_3	89.97 mg/g	500 mg/L	7.0	303	0.75	Langmuir	Pseudo-second-order	25
CTAB modified graphene	Cr(VI)	21.57 mg/g	20-100 mg/L	2.0	298	1	Langmuir	Pseudo-second-order	85

SiO_2/graphene	Pb(II)	113.6 mg/g	20 mg/L	6.0	298	1	Langmuir	Pseudo-second-order	86
Functionalized graphene (GNS^{PF6})	Pb(II)	406.4 mg/g		5.1		4	Langmuir, Freundlich	Pseudo-second-order	87
Functionalized graphene (GNS^{PF6})	Cd(II)	73.42 mg/g		6.2		4	Langmuir, Freundlich	Pseudo-second-order	87
Functionalized graphene (GNS^{C8P})	Pb(II)	74.18 mg/g		5.1		4	Langmuir, Freundlich	Pseudo-second-order	87
Functionalized graphene (GNS^{C8P})	Cd(II)	30.05 mg/g		6.2		4	Langmuir, Freundlich	Pseudo-second-order	87
GO	Pb(II)	367 mg/g	5-300mg/L	6.8	298±2	24	Langmuir		75
GO	U(VI)	299 mg/g		4.0	Room temp.	4	Langmuir		92
GO	Zn(II)	30.1±2.5 mg/g		5.6					95
GO	Cd(II)	14.9±1.5 mg/g		5.6					95
GO	Pb(II)	35.6±1.3 mg/g		5.6					95

GO	Cu(II)	117.5mg/g	25-250mg/L	5.3		2.5	Freundlich		73
GO	Pb(II)	692.66 mg/g	5-300 mg/L	7.0±0.5	298±5	24	Langmuir		96
GO	Cu(II)	294 mg/g		5.0	298	2	Langmuir	Pseudo-second-order	94
GO	Zn(II)	345 mg/g		5.0	298	2	Langmuir	Pseudo-second-order	94
GO	Cd(II)	530 mg/g		5.0	298	2	Langmuir	Pseudo-second-order	94
GO	Pb(II)	1119 mg/g		5.0	298	2	Langmuir	Pseudo-second-order	94
GO	Zn(II)	246 mg/g	10-100 mg/L	7.0±0.1	293		Langmuir	Pseudo-second-order	93
		236 mg/g			303				
		225 mg/g			318				

GO aerogel	Cu(II)	17.73 mg/g	50-75 mg/L	6.3	283	0.5	Langmuir	Pseudo-second-order	97
		19.65 mg/g			298				
		29.59 mg/g			313				
Graphene/c-MWCNT	Pb(II)	104.9 mg/g	50 mg/L		Room temp.	120			88
Graphene/c-MWCNT	Hg(II)	93.3 mg/g	50 mg/L		Room temp.	120			88
Graphene/c-MWCNT	Ag(II)	64.0 mg/g	50 mg/L		Room temp.	120			88
Graphene/c-MWCNT	Cu(II)	33.8 mg/g	50 mg/L		Room temp.	120			88
Graphene/c-MWCNT	Pb(II)	44.5 mg/g	50 mg/L		Room temp.	120			88
Graphene/c-MWCNT	Hg(II)	75.6 mg/g	50 mg/L		Room temp.	120			88
Graphene/c-MWCNT	Ag(II)	46.0 mg/g	50 mg/L		Room temp.	120			88
Graphene/c-MWCNT	Cu(II)	9.8 mg/g	50 mg/L		Room temp	120			88

rGO-Fe(O)	As(II)	37.3 mg/g	2-6 mg/L	7.0	298	1	Langmuir	Pseudo-second-order	120
rGO-Fe_3O_4	As(III)	21.2 mg/g	2-6 mg/L	7.0	298	1	Langmuir	Pseudo-second-order	117
rGO-Fe(O)/Fe_3O_4	As(III)	44.4 mg/g	2-6 mg/L	7.0	298	1	Langmuir	Pseudo-second-order	117
rGO-Fe(O)/Fe_3O_4	Cr(III)	31.1 mg/g	2-6 mg/L	7.0	298	1	Langmuir		117
rGO-Fe(O)/Fe_3O_4	Hg(VI)	22.0 mg/g	2-6 mg/L	7.0	298	1	Langmuir		117
rGO-Fe(O)/Fe_3O_4	Pb(II)	19.7 mg/g	2-6 mg/L	7.0	298	1	Langmuir		117
rGO-Fe(O)/Fe_3O_4	Cd(II)	1.91 mg/g	2-6 mg/L	7.0	298	1	Langmuir		117
PAS-GO	Pb(II)	312.5 mg/g	10-400 mg/L	6.0	303	7	Langmuir	Pseudo-second-order	99
As-GO	Pb(II)	119.05 mg/g	10-400 mg/L	6.0	303	7	Langmuir	Pseudo-second-order	99

GO	Pb(II)	204.04 mg/g	10-400 mg/L	6.0	303	7	Langmuir	Pseudo-second-order	99
GO	Co(II)	116.35 mg/g	30 mg/L	6.0	298	12	Langmuir	Pseudo-second-order	72
GO Foam	Cd(II)	252.6 mg/g	50 mg/L	10	Room temp.	1	Langmuir		100
GO Foam	Zn(II)	326.4 mg/g	5 mg/L	10	Room temp.	1	Langmuir		100
GO Foam	Pb(II)	381.1 mg/g	5 mg/L	10	Room temp.	1	Langmuir		100
GO Foam	Fe(III)	587 mg/g	50 mg/L	10	Room temp.	1	Langmuir		100
NZVI-rGO	As(III)	35.83 mg/g		7.0(±0.25)	297(±0.5)	2	Langmuir	Pseudo-second-order	118
NZVI-rGO	As(V)	29.04 mg/g		7.0(±0.25)	297(±0.5)	2	Langmuir	Pseudo-second-order	118

Magnetic cyclodextrin-chitosan/GO	Cr(VI)	61.31 mg/g 67.34 mg/g 67.66 mg/g	50 mg/L	3.0	303 313 321		Langmuir	Pseudo-second-order	113
Calcium alginate/GO	Cu(II)	60.24 mg/g			Room temp.	1.5	Langmuir	Pseudo-second-order	114
Poly(N-vinylcarbazole)-GO	Pb(II)	887.98 mg/g	5-300 mg/L	7.0±0.5	298±5	24	Langmuir		96
Polypyrrole-rGO	Hg(II)	980 mg/g	50-250	3.0	298	3	Langmuir, Freundlich	Pseudo-second-order	122
Magnetite-rGO	As(V)	13.10 mg/g	3-7 mg/L	7.0	293	2	Langmuir	Pseudo-second-order	121
Magnetite-rGO	As(III)	10.20 mg/g	3-7 mg/L	7.0	293	2	Langmuir	Pseudo-second-order	121
rGO-Ag	Hg(II)	9.50 mg/g	1 mg/L		303(±2)			Pseudo-second-order	120
rGO-MnO_2	Hg(II)	9.53 mg/g	1 mg/L		303(±2)			Pseudo-second-order	120

$CoFe_2O_4$	Pb(II)	299.4 mg/g	20 mg/L	5.3	298	2	Langmuir	Pseudo-second-order	119
$CoFe_2O_4$	Hg(II)	157.9 mg/g	5 mg/L	4.6	298	2	Langmuir	Pseudo-second-order	119
Graphene/MgAl-layered	Cr(VI)	183.82 mg/g	50-250 mg/L	2.0		24	Freundlich	Pseudo-second-order	89
Double hydroxides									
GO/ferric hydroxide	As(V)	23.78 mg/g	0.5-20 mg/L	4.0-9.0	Room temp.	24	Langmuir	Pseudo-second-order	104
Magnetite/GO	Co(II)	12.98 mg/g			303.2	24	Langmuir	Pseudo-second-order	105
		17.58 mg/g			323.2				
		22.70 mg/g			343.2				
GO/chitosan	Pb(II)	99 mg/g	50 mg/L		Room temp.		Langmuir		110
Chitosan/GO	Au(III)	1076.649 mg/g	80-500 mg/L		Room temp.	16	Langmuir	Pseudo-second-order	23
Chitosan/GO	Pb(II)	216.920 mg/g	80-500 mg/L		Room temp.	16	Langmuir	Pseudo-second-order	23

Fe_30_4/GO	U(VI)	69.49 mg/g	$2.25^{x}10^{5}$ - $2.24^{x}10^{-5}$ mol/L	5.5±0.1	303	24	Langmuir	Pseudo-second-order	108
GO-chitosan composite hydrogen	Cu(II)	70 mg/g	0-120 mg/L	5.1	294±1	10	Freundlich		157
GO-chitosan composite hydrogen	Pb(II)	90 mg/g	0-120 mg/L	4.9	294±1	4	Freundlich		157
Magnetic chitosan/GO	Pb(II)	76.94 mg/g		5.1	303± (0.2)	1	Langmuir	Pseudo-second-order	112
Polypyrrole/GO	Cr(VI)	9.55 mmol/g					Langmuir	Pseudo-second-order	106
GO-FeOOH	As(V)	73.42 mg/g		7.0	298		Langmuir	Pseudo-second-order	107
GO@sepiolite	U(VI)	161.3 mg/g	10-50mg/L	5.0	298		Langmuir		111
GO-TiO_2	Zn(II)	88.9±3.3 mg/g		5.6					95

GO-TiO_2	Cd(II)	72.8±1.6 mg/g		5.6					95
GO-TiO_2	Pb(II)	65.6±2.7 mg/g		5.6					95
GO-$ZrO(OH)_2$	As(II)	95.15 mg/g	2-80 mg/L	7.0±0.2	298.5±0.2	0.25	Langmuir	Pseudo-second-order	103
GO-$ZrO(OH)_2$	As(V)	84.89 mg/g	2-80 mg/L	7.0±0.2	298.5±0.2	0.25	Langmuir	Pseudo-second-order	103
Sulfonted magnetic GO composite	Cu(II)	50.68 mg/g	73.71 mg/L	5.0	283.2	6	Langmuir	Pseudo-second-order	102
		56.86 mg/g			303.2				
		63.67 mg/g			323.2				
EDTA modified GO	Pb(II)	525 mg/g	5-300 mg/L	6.8	298±2	24	Langmuir		75
Poly(amidoamine) modified GO	Fe(III)	0.5312 mmol/g	0.0193 mmol/L		Room temp.	24			103
Poly(amidoamine) modified GO	Cr(III)	0.0798 mmol/g	0.0193 mmol/L		Room temp.	24			103
Poly(amidoamine) modified GO	Zn(II)	0.2024 mmol/g	0.0193 mmol/L		Room temp.	24			103

Poly(amidoamine) modified GO	Pb(II)	0.0513 mmol/g	0.0193 mmol/L		Room temp.	24			103
Poly(amidoamine) modified GO	Cu(II)	0.1368 mmol/g	0.0193 mmol/L		Room temp.	24			103
FrGO	Cu(II)	18.60 mg/g	0-30 mg/L	4-6	296±1	24	Langmuir	Pseudo-second-order	115
FGO	Cu(II)	82.91 mg/g	0-30 mg/L	4-6	296±1	24	Langmuir	Pseudo-second-order	115
FGO	Cd(II)	106.3 mg/g		6.0±0.1	303		Langmuir		19
		153.6 mg/g			313				
		167.5 mg/g			333				
FGO	Co(II)	68.2 mg/g		6.0±0.1	303		Langmuir		19
		69.4 mg/g			313				
		79.8 mg/g			333				
Graphene/Fe	Cr(VI)	162 mg/g	25-125 mg/L	4.25	293	4	Langmuir, Freundlich	Pseudo-second-order	90

Graphene/ δ-MnO_2	Ni(II)	46.55 mg/g 60.31 mg/g 66.01 mg/g	10-100 mg/L		298 308 318	3	Langmuir	Pseudo-second-order	61
Graphene/ δ-MnO_2	Cu(II)	1637.965 µmol/g		6.0	298±2	2	Langmuir	Pseudo-second-order	61
Graphene/ δ-MnO_2	Pb(II)	773.65 µmol/g		6.0	298±2	2	Langmuir	Pseudo-second-order	61
Graphene/$Fe@Fe_2O_3$ @Si-S-O	Cr(VI)	1.03 mg/g	1 g/L	7.0				Pseudo-second-order	18
Graphene/ $Mn_x^{2+}Fe_{2=x}^{3+}O_4^{2-}$	As(III)	14.42 mg/g	1-8 g/L	7.0±0.1	300±1	2.5	Langmuir	Pseudo-second-order	91

Table 3. Summary of reported results for dyes removal from aqueous solution and wastewater by graphene based adsorbents

Adsorbent	Adsorbate	Adsorption Capacity	Conc.	pH	Temp. (K)	Contact time (h)	Models applicable		Reference
							Isotherm	Kinetic	
GO/Cellulose (GOCB)	Malachite Green	30.091 mg/g	10 mg/L	7.0	298	5	Langmuir	Pseudo-second-order	141
Magnetic cyclodextrin/ GO (MCGO)	Methylene blue	261.78 mg/g	100 mg/L	10	303	0.83	Langmuir	Pseudo-second-order	154
MgO ducked multi-layered graphene (MDMLD)	Safranin O	3.92×10^{-4} mol/g	4.0×10^{-4} M	2-12	-	2	Langmuir	Pseudo-second-order	143
GO-sodium alginate (GO-SA)	Methylene blue	833.3 mg/g	0.1mol/L	-	303	12	Langmuir and Freundlich	Pseudo-second-order and intra-particle diffusion	159
Polydopamine layer coated GO (PD5%/GO)	Methylene blue	1.3 g/g	-	8.5	-	-	Langmuir	-	161
Polydopamine layer coated GO (PD15%/GO)	Methylene blue	1.89 g/g	-	8.5	-	-	Langmuir	-	161

Polydopamine layer coated GO (PD35%/GO)	Methylene blue	1.7 g/g	-	8.5	-	-	Langmuir	-	161
Polydopamine layer coated GO (PD70%/GO)	Methylene blue	0.6 g/g	-	8.5	-	-	Langmuir	-	161
GO_1	Methylene blue	40.6 mg/g	600 mg/dm^3	-	-	0.083	Langmuir	Pseudo-second-order	139
GO_2	Methylene blue	157.6 mg/g	600 mg/dm^3	-	-	0.083	Langmuir	Pseudo-second-order	139
GO_3	Methylene blue	334.7 mg/g	600 mg/dm^3	-	-	0.083	Langmuir	Pseudo-second-order	139
GO_4	Methylene blue	454.5 mg/g	600 mg/dm^3	-	-	0.083	Langmuir	Pseudo-second-order	139
GO_5	Methylene blue	513.9 mg/g	600 mg/dm^3	-	-	0.083	Langmuir	Pseudo-second-order	139
GO_6	Methylene blue	570.4 mg/g	600 mg/dm^3	-		0.083	Langmuir	Pseudo-second-order	139
GO	Basic Blue 41(BB41)	1429 mg/g	50 mg/L	-	298	1	Langmuir	Pseudo-second-order	138

GO	Basic Red 18 (BR18)	1250 mg/g	50 mg/L	-	298	1	Langmuir	Pseudo-second-order	138
GO	Basic Red 46(BR46)	476 mg/g	50 mg/L	-	298	1	Langmuir	Pseudo-second-order	138
GO-Zeolite	Rhodamine B	55.56 mg/g	1-500 mg/dm^3	-	-	1	Langmuir	Pseudo-second-order	109
Carboxy-GO/Zeolite	Rhodamine B	67.56 mg/g	1-500 mg/dm^3	-	-	1	Langmuir	Pseudo-second-order	109
Graphene oxide/ chitosan/silica fibre	Congo red	294.12 mg/g	80mg/L	3.0	293	-	Langmuir	Pseudo-first-order	158
rGO-sodium alginate (rGO-SA)	Methylene blue	192.3 mg/g	0.1mol/L		303	12	Langmuir and Freundlich	Pseudo-second-order and intra-particle diffusion	159
rGO	Methyl green	3.163 mmol/g	-	5	298	1	Langmuir	Pseudo-second-order	145
rGO	Methylene blue	302.11 mg/g	300 mg/L	7	-	48	Langmuir	Pseudo-second-order	144
rGO	Acid Red	28.51 mg/g	50 mg/L	7	-	48	Langmuir	Pseudo-second-order	144

GO	Methylene blue	243.65 mg/g	40 – 120 mg/L	6	298	5	Langmuir	Pseudo-second-order	81
GO	Methyl Green	4821 mmol/g	-	4.0	398	1	Langmuir	Pseudo-second-order	137
		5.496 mmol/g		5.0					
		6.167 mmol/g		6.0					
		6.628 mmol/g		7.0					
		7.613 mmol/g		9.0					
Magnetic graphene oxide (MGO)	Methylene blue	64.23 mg/g	90 mg/L	-	298	6.75	Langmuir	Pseudo-second-order	160
Magnetic graphene oxide (MGO)	Orange G	20.85 mg/g	60mg/L	-	298	6.75	Langmuir	Pseudo-second-order	160
Graphene-chitosan	Methylene blue	390 mg/g	0-80 mg/L	6.5	294±1	58	-	-	111
Graphene-chitosan	Eosin Y	326 mg/g	0-80 mg/L	7.0	294±1	36	-	-	111
Graphene/sand	Rhodamine 6G	75.4 mg/g	-	-	303±2	6	-	Pseudo-second-order	127

Magnetic β-cyclodextrin-chitosan/GO	Methylene blue	84.32 mg/g	-	-	298	-	Langmuir	Pseudo-second-order	112
GO/calcium alginate	Methylene blue	181.81 mg/g	30-80 mg/L	-	298	5	Langmuir	Pseudo-second-order	135
Graphene-SO_3H/Fe_3O_4	Safrainin T	199.3 mg/g	20-250 mg/L	6.0	Room temp	-	Langmuir	Pseudo-second-order	93
Graphene-SO_3H/Fe_3O_4	Neural red	216.8 mg/g	20-250 mg/L	6.0	Room temp	-	Langmuir	Pseudo-second-order	93
Graphene-SO_3H/Fe_3O_4	Victoria Blue	200.6 mg/g	20-250 mg/L	6.0	Room temp	-	Langmuir	Pseudo-second-order	93
Graphene/$CoFe_2O_4$	Methyl green	203.51 mg/g	50-400 mg/L	-	298	-	Langmuir	Pseudo-second-order	134
		258.39 mg/g			313				
		312.80 mg/g			323				
Graphene/Fe_3O_4	Pararosaniline	1988.23 mg/g	20-60 mg/L	6.6± 0.2	298	1	Langmuir	Pseudo-second-order	126
rGO-based hydrogel	Methylene blue	7.85 mg/g	0.5-10 mg/L	6.4	298	2	Freundlich	Pseudo-second-order	146

rGO-based hydrogel	Rhodamine B	29.44 mg/g	0.5-10 mg/L	6.4	298	2	Freundlich	Pseudo-second-order	146
GO	Acridine orange	1428 mg/g	0.1 g/L	-	Room temp	3	Langmuir	-	136
Graphene	Methylene blue	153.85 mg/g	20-120 mg/L	10.0	293		Langmuir	Pseudo-second-order	23
		185.19 mg/g			313				
		204 mg/g			333				
Graphene sponge	Methylene blue	184 mg/g	2×10^{-4} mol/L	-	298	4	-	-	20
Graphene sponge	Rhodamine B	72.5 mg/g	2×10^{-4} mol/L	-	298	4	-	-	20
Graphene sponge	Methyl Orange	11.5 mg/g	2×10^{-4} mol/L	-	298	24	-	-	20
Magnetite@ graphene	Congo red	33.66 mg/g	-	-	298±0.5 2	-	Langmuir	Pseudo-second-order	124

Magnetite@ graphene	Methylene blue	45.27 mg/g	-	-	298± 0.5	-	Langmuir	Pseudo-second-order	124
In situ rGO	Acridine orange	3333mg/g	0.1 g/L	-	Room	3	Langmuir	-	136
Graphene/c-MWCNT	Rhodamine B	150.2	20 mg/L	-	Room temp	-		Pseudo-second-order	136
Graphene/c-MWCNT	Methylene blue	191.0	20 mg/L	-	Room temp	--	-	Pseudo-second-order	136
Graphene/c-MWCNT	Fuchsine	180.8	20 mg/L	-	Room temp	-	-	Pseudo-second-order	136
Graphene/c-MWCNT	Acid Fuchsine	35.8	20 mg/L	-	Room temp	-	-	Pseudo-second-order	136
Graphene-CNT	Methylene blue	81.97	10-30 mg/L	-	-	3	Freundlich	Pseudo-second-order	129
Graphene/sand	Rhodamine 6G	55 mg/g	5 mg/L	-	303±2	8	-	Pseudo-second-order	128
$Fe_3O_4.SiO_2$	Methylene blue	97 mg/g	-	-	298	-	Langmuir	Pseudo-second-order	142

		102 mg/g			318				
		111.1 mg/g			333				
Polystyrene@Fe_3O_4@GO	Rhodamine B	13.8 mg/g	0-150 mg/L	-	Room temp	24	-	-	152
rGO@ZnO	Rhodamine B	32.6 mg/g	4-750 mg/L	-	293	-	-	-	150
rGO-titanate	Methylene blue	83.26 mg/g	10 mg/L	-	-		-	Pseudo-second-order	149
Magnetic chitosan/GO	Methyl blue	95.31 mg/g	60-200 mg/L	5.3	303	1	Langmuir	Pseudo-second-order	155
Magnetic chitosan/GO	Methylene blue	180.83 mg/g	50-100 mg/L	-	303± 0.2	-	Langmuir	Pseudo-second-order	156
rGO	Orange G	5.98 mg/g	1-60 mg/L	-	-	-	Langmuir	Pseudo-second-order	178
Graphene	Cationic red X-GRL	217.39 mg/g	20-140 mg/L		288	24	Langmuir	Pseudo-second-order	92
		227.39 mg/g			313				
		238 mg/g			333				

Graphene	Methylene blue	1.52 g/g	5 mg/L		303	96	-	-	123
GO	Methylene blue	17.3 mg/g	10-50mg/L	10.0	-	-	Langmuir	Pseudo-second-order	78
GO	Methyl Violet	2.47 mg/g	10-50mg/L	6.0	-	-	Langmuir	Pseudo-second-order	78
GO	Rhodamine B	1.24 mg/g	1-10 mg/L	6.0	-	-	Freundlich	Pseudo-second-order	78
Graphene/Fe_3O_4	Fuchsine	89.4 mg/g	20-60 mg/L	6.6± 0.2	298	1	Langmuir	Pseudo-second-order	59
Graphene/magnetite	Methylene blue	43.82 mg/g	10-25 mg/L	-	298	-	Langmuir	Pseudo-second-order	129
$CoFe_2O_4$-functionlized graphene	Methyl orange	71.54 mg/g	10mg/L	-	-	-	-	Pseudo-second-order	135
Magnetite/rGO	Rhodamine B	13.15 mg/g	0.5-4 mg/L	7.0	298	2	Langmuir Freundlich	Pseudo-second-order	151
Magnetite/rGO	Malachite green	22.0 mg/g	0.5-4 mg/L	7.0	298	2	Langmuir Freundlich	Pseudo-second-order	151